JOURNAL OF BIOMOLECULAR STRUCTURE AND DYNAMICS
https://doi.org/10.1080/07391102.2022.2116600

Design, synthesis, spectroscopic characterizations, *in vitro* pancreatic lipase as well as tyrosinase inhibition evaluations and *in silico* analysis of novel aryl sulfonate-naphthalene hybrids

Adem Korkmaz[a], Gülbin Kurtay[b], Esin Kaya[c] and Ercan Bursal[a]

[a]Faculty of Health Sciences, Muş Alparslan University, Muş, Turkey; [b]Department of Chemistry, Faculty of Science, Ankara University, Ankara, Turkey; [c]Faculty of Education, Muş Alparslan University, Muş, Turkey

Communicated by Ramaswamy H. Sarma

ABSTRACT

One of the primary purposes of this study is to synthesize new aryl sulfonate-naphthalene hybrid structures possessing divergent electron-withdrawing and electron-releasing functional groups. Following the improved reaction conditions, we successfully gathered ten distinct sulfonate derivatives (**3a-j**) with good yields. The synthesized naphthalene-based sulfonate derivatives were then characterized using appropriate analytical methods (FT-IR, ^{1}H-NMR, ^{13}C-NMR, HRMS, and elemental analysis). Additionally, *in vitro* and *in silico* enzyme inhibitory properties of the prepared aryl sulfonate-naphthalene hybrid structures were evaluated against pancreatic lipase and tyrosinase enzymes. Corresponding *in vitro* enzyme activity investigations revealed that the produced compounds inhibit pancreatic lipase and tyrosinase enzymes significantly. According to the lowest IC_{50} values, **3h** (95.3 ± 4.0 μM) demonstrated the most effective inhibition against pancreatic lipase, whereas **3a** (40.8 ± 3.3 μM) was found as the most effective inhibition against the tyrosinase. According to *in silico* studies, **3a** exhibited the highest affinity value (−9.9 kcal/mol) against pancreatic lipase, whereas **3f** demonstrated the best affinity value (−8.7 kcal/mol) against tyrosinase.

Furthermore, we investigated various structural and physicochemical properties of the target molecules, namely frontier orbital' (HOMO, LUMO, and bandgap) energies (including their corresponding contour plots), global reactivity descriptors (ionization energy and electron affinity), and electronegativity values gathered from ground-state (GS) density functional theory (DFT) calculations. These investigations demonstrated that the observed electrostatic interactions effectively contributed to the studied molecules' experimentally demonstrated enzyme inhibition potential. Also, ADMET studies were evaluated to enlighten the molecular interactions of the compounds with the enzymes.

ARTICLE HISTORY
Received 24 May 2022
Accepted 18 August 2022

KEYWORDS
Enzyme inhibition; molecular docking; naphthalene-based sulfonate derivatives; pancreatic lipase; tyrosinase

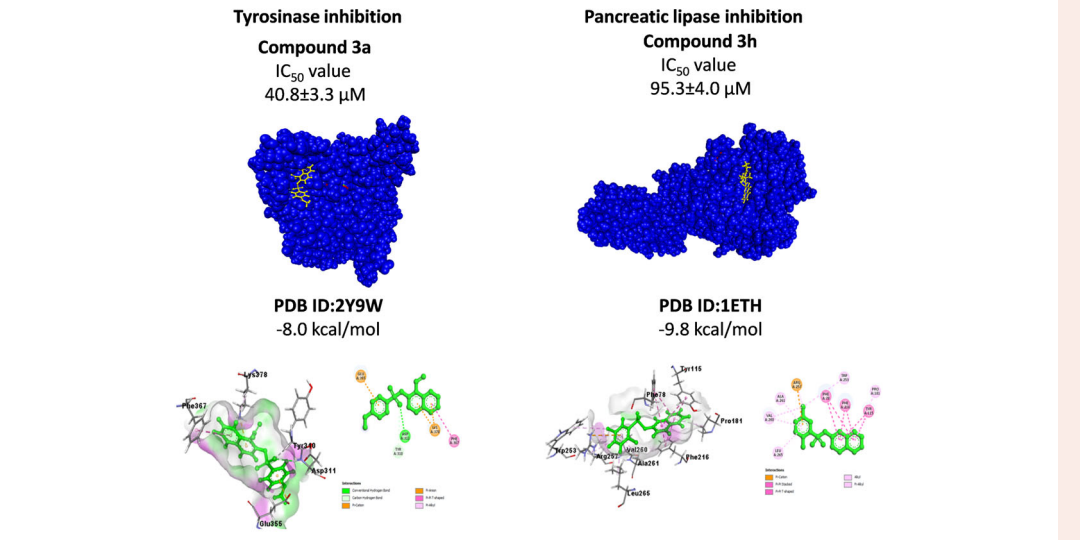

CONTACT Adem Korkmaz a.korkmaz@alparslan.edu.tr; Ercan Bursal e.bursal@alparslan.edu.tr Faculty of Health Sciences, Muş Alparslan University, Muş 49250, Turkey

Supplemental data for this article can be accessed online at https://doi.org/10.1080/07391102.2022.2116600.

1. Introduction

In the relevant scientific discipline, there is a rising interest in enzyme inhibition screening and detection investigations for identifying new reliable medications. In this study, we sought to decipher the possible enzyme inhibitor characteristics of newly produced compounds against tyrosinase and pancreatic lipase enzymes. Designing the synthetic compounds for enzyme inhibitors is a hot topic research area and has been the subject of many published papers (Akocak et al., 2021; Behl et al., 2021; Çakmak et al., 2022; Gümüş et al., 2022). Although many synthetic compounds have been screened for their inhibitory enzyme activities, the number of approved drugs for enzyme inhibitors remains limited and does not meet the needs of the drug industry (Cetin et al., 2021; Demir et al., 2020; Turkan et al., 2019).

Tyrosinase (mono/polyphenol oxidase) is a critical enzyme family in the melanin biosynthesis pathway responsible for skin and hair pigmentation (Song et al., 2021). Melanin has functions for skin protection against harmful ultraviolet radiation and prevention of cancer development. However, overexpression of melanin leads to several skin diseases (Kim et al., 2016). Thus, tyrosinase inhibition is crucial in preventing the harmful results of excessive melanin production. Tyrosinase inhibitors have been utilized as skin lightening agents in cosmetics. Many tyrosinase inhibitors derived from natural and synthetic sources have recently been found. Among the several substances examined, kojic acid, ascorbic acid, arbutin, and hydroquinone were acknowledged as standard tyrosinase enzyme inhibitors (Pillaiyar et al., 2017).

Pancreatic lipase is a digestive enzyme that aids in the breakdown of dietary lipids in the gastrointestinal tract. Obesity is thought to be caused chiefly by excess fat accumulated in the body (Kumar & Chauhan, 2021). Obesity is associated with several health issues or metabolic diseases, including hypertension, diabetes mellitus, cardiovascular issues, and some forms of cancer (Li et al., 2021). Pancreatic lipase inhibitors have been used to treat obesity because they reduce fat absorption via the small intestine (Liu et al., 2020). Among the many screened inhibitor compounds, orlistat has been confirmed and used as an effective obesity drug with a potent pancreatic lipase inhibitor (George et al., 2021).

Naphthalene derivatives have been extensively studied with various applications (Ciupak et al., 2021; Erdoğan et al., 2021; Wang et al., 2020). Some potent inhibitors (**I**-**VI**) of the naphthalene derivatives shown in Scheme 1 were investigated previously. It has been reported that the anticancer activities of synthesized 1,5-N,N′-substituted-2-(substituted naphthalenesulfonyl) glutamamide derivatives (**I**, **II**) were evaluated against Ehrlich Ascites Carcinoma (EAC) cells in Swiss Albino mice as anticancer agents (Halder et al., 2010). The emphasis of interest has shifted to investigations on synthesizing modified naphthalene-based derivatives (**III**) with pharmacological characteristics, such as acetylcholinesterase and paraoxonase 1 inhibition (Shirinzadeh et al., 2022). Carbonic anhydrase inhibition properties of imino-methyl-naphthalen-2-ol (**IV**) were investigated in a recent study (Abbas et al., 2018). Furthermore, hybrid compounds containing naphthalene moiety (**V**) as potent antioxidants and lipoxygenase inhibitors were synthesized, and molecular modeling studies were accordingly reported (Ali et al., 2020). It was encountered that naphthalene analogs (**VI**) displayed their antimitotic effects in human cancer cells by disrupting the microtubule network, followed by G2/M arrest of the cell cycle (Maya et al., 2005). Another study reported that acetone O-(4 chlorophenylsulfonyl) oxime, a sulfonated derivative, has a significant potential for phytoremediation studies (Yetişsin & Kardeş, 2022).

In this study, we synthesized ten novel naphthalene-based sulfonated derivatives by a triethylamine (TEA)-mediated mild reaction process. Then, the synthesized compounds were screened for their *in vitro* as well as *in silico* pancreatic lipase and tyrosinase inhibitory activities. Moreover, the density functional theory (DFT) and ADMET (absorption, distribution, metabolism, excretion, and toxicity) predictions of the naphthalene-based sulfonate derivatives were also performed to elucidate their physicochemical properties and reactivity patterns in order to describe their potent applicabilities.

2. Experimental

2.1. Materials and instrumentation

N,*N*-Dimethylformamide (DMF, Sigma-Aldrich) was used by purified in a vacuum with 4Å molecular sieves. All the other required reagents and solvents, including Benzene (99%), 4-Chlorobenzenesulfonyl chloride (97%), *n*-Hexane (95%), 2-Hydroxynaphthalene (98%), 2-Hydroxynaphthaldehyde, 4-Methoxybenzenesulphonyl chloride (99%), 4-Fluorobenzenesulphonyl chloride (98%), 2-Naphthylsulphonyl chloride (99%), 2,5-Dichlorobenzenesulphonyl chloride (98%), 2,4,6-Triisopropylbenzenesulphonyl chloride (99%), 4-Bromobenzenesulphonyl chloride (98%), 2,4,6-Trimethylbenzene sulphonyl chloride (97%), and Triethylamine (TEA) (99.5%) were purchased from Sigma-Aldrich and used without further purification processes. The mushroom tyrosinase and porcine pancreatic lipase enzyme sources were purchased from Sigma-Aldrich.

The melting points were measured by a thermo-scientific capillary. ^{1}H (400 MHz) and ^{13}C (100 MHz) NMR spectra were gathered using a Bruker DRX-400. High-resolution mass spectra (HRMS) data were collected using Agilent Q-TOF Mass Spectrometer (Acquisition SW Version (6200 series TOF/6500 series Q-TOF B.08.00 (B8058.0)) in ESI mode. Elemental analysis studies were conducted with LECO CHNS-932 Elementary Chemical Analyzer. Thermo multi-scan microplate spectrophotometer was used for enzyme kinetic measurements.

2.2. General synthesis of naphthalene-bearing sulfonate derivatives

Naphthalene-based sulfonate derivatives were prepared using a similar method previously described (Korkmaz, 2022; Korkmaz & Bursal, 2022a). For this purpose, a two-necked flask was filled with 2-hydroxynaphthalene or 2-hydroxynaphthaldehyde (3.425 mmol), TEA (4.110 mmol, 0.570 mL), and DMF (2.5 mL). The flask content was cooled in an ice

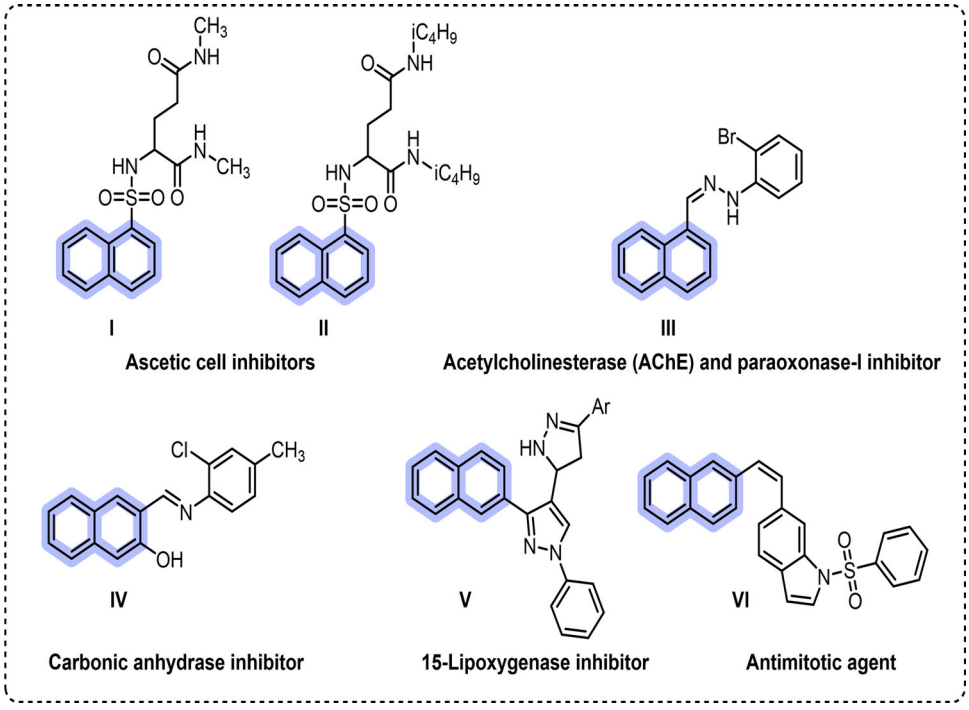

Scheme 1. Biological agents bearing naphthalene moiety.

bath and the reaction was initiated by the steady addition (in 2–3 min) of the corresponding sulfonyl chloride (3.425 mmol). The addition of sulfonyl chloride derivatives were terminated (approx. in 5 min). The formation of a colloidal solution was observed and the reaction vessel was scanned with Thin Layer Chromatography (TLC), and it was continued for 60 min by controlled TLC. The crude product was poured into water (20 mL). The residue was separated by vacuum suction, repeatedly washed with distilled water, and dried into a desiccator. The recrystallization was made in the benzene-hexane mixture (1:5) to afford the desired compounds in good yields.

2.2.1. 1-Formylnaphthalen-2-yl 4-methoxybenzenesulfonate (3a)

Light cream powder (benzene-hexane (1:5)); m.p 110–112 °C; mol. wt: 342.06; yield 64%. FT-IR (KBr, cm^{-1}) ν: 3103.53, 3060.71, 3007.14(sp^2 C-H), 1686.95 (ArHC = O), 1593.37, 1577.08, 1491.65 (Ar C-C), 1370.41 ($ArSO_2OAr$ band), 1171.92 ($ArSO_2OAr$ band). ^{1}H NMR (400 MHz, $CDCl_3$), δ/ppm: 10.42 (s, 1H, CHO), 9.16 (d, 1H, J = 8.60 Hz, Ar-H), 8.07 (d, 1H, J = 9.00 Hz, Ar-H), 7.88 (d, 1H, J = 8.10 Hz, Ar-H), 7.77 (d, 2H, J = 8.90 Hz, Ar-H), 7.70–7.64 (m, 1H, Ar-H), 7.62–7.56 (m, 1H, Ar-H), 7.36 (d, 1H, J = 9.00 Hz, Ar-H), 6.99 (d, 2H, J = 8.90 Hz, Ar-H), 3.90 (s, 3H, Ar-OCH_3). ^{13}C NMR (100 MHz, $CDCl_3$), δ/ppm: 189.9 (Ar-CHO), 164.8 (Ar-C), 153.2 (Ar-C), 136.5 (Ar-C), 132.1 (Ar-C), 130.8 (2 units of Ar-C), 130.6 (Ar-C), 129.8 (Ar-C), 128.3 (Ar-C), 127.1 (Ar-C), 125.7 (Ar-C), 125.3 (Ar-C), 123.0 (Ar-C), 121.5 (Ar-C), 114.5 (2 units of Ar-C), 55.8 (Ar-OCH_3). HRMS (ESI) m/z: calculated for $C_{18}H_{14}O_5S$ $[M+H]^+$: 343.0600; found: 343.06307. Anal. Cald. For $C_{18}H_{14}O_5S$: C, 63.15; H, 4.12; S, 9.37; Found: C, 62.85; H, 3.66; S, 8.92.

2.2.2. 1-Formylnaphthalen-2-yl 4-chlorobenzenesulfonate (3b)

Light cream powder (benzene-hexane (1:5)); m.p 133–135 °C; mol. wt: 346.01; yield 85%. FT-IR (KBr, cm^{-1}) ν: 3092.85 (sp^2 C-H), 1685.73 (ArHC = O), 1571.57, 1508.16, 1438.51 (Ar C-C), 1352.79 ($ArSO_2OAr$), 1179.75 ($ArSO_2OAr$), 1087.52 (Ar-Cl). ^{1}H NMR (400 MHz, DMSO-d6), δ/ppm: 10.34 (s, 1H, CHO), 8.94 (d, 1H, J = 8.60 Hz, Ar-H), 8.29 (d, 1H, J = 9.0 Hz, Ar-H), 8.03 (d, 1H, J = 8.0 Hz, Ar-H), 7.93–7.87 (m, 2H, Ar-H), 7.74–7.68 (m, 3H, Ar-H), 7.65–7.60 (m, 1H, Ar-H), 7.30 (d, 1H, J = 9.00 Hz, Ar-H).^{13}C NMR (100 MHz DMSO-d6), δ/ppm: 190.0 (Ar-CHO), 152.0 (Ar-C), 141.3 (Ar-C), 137.5 (Ar-C), 132.4 (Ar-C), 132.3 (Ar-C), 130.8 (2 units of Ar-C), 130.7 (2 units of Ar-C), 130.4 (Ar-C), 130.3 (Ar-C), 129.2 (Ar-C), 127.8 (Ar-C), 125.1 (Ar-C), 123.2 (Ar-C), 121.6 (Ar-C). HRMS (ESI) m/z: calculated for $C_{17}H_{11}ClO_4S$ $[M+H]^+$: 347.0100; found: 347.01257. Anal. Cald. For $C_{17}H_{11}ClO_4S$: C, 58.88; H, 3.20; S, 9.25; Found: C, 58.62; H, 3.49; S, 9.14.

2.2.3. 1-Formylnaphthalen-2-yl 4-bromobenzenesulfonate (3c)

Light cream powder (benzene-hexane (1:5)); m.p 135–137 °C; mol. wt: 389.96; yield 85%. FT-IR (KBr, cm^{-1}) ν: 3092.85(sp^2 C-H), 1685.67 (ArHC = O), 1571.50, 1508.74 (Ar C-C), 1352.71 ($ArSO_2OAr$), 1177.46, ($ArSO_2OAr$). ^{1}H NMR (400 MHz, $CDCl_3$), δ/ppm: 10.47 (s, 1H, CHO), 9.17 (d, 1H, J = 8.60 Hz, Ar-H), 8.10 (d, 1H, J = 8.90 Hz, Ar-H), 7.90 (d, 1H, J = 8.10 Hz, Ar-H), 7.79–7.68 (m, 5H, Ar-H), 7.61 (t, 1H, J = 7.20 Hz, Ar-H), 7.34 (d, 1H, J = 9.00 Hz, Ar-H). ^{13}C NMR (100 MHz, $CDCl_3$), δ/ppm: 189.6 (Ar-CHO), 152.7 (Ar-C), 136.7 (Ar-C), 133.3 (2 units of Ar-C), 133.0 (Ar-C), 132.2 (Ar-C), 130.7 (Ar-C), 130.6 (Ar-C), 130.1 (Ar-C), 129.9 (2 units of Ar-C), 128.4 (Ar-C), 127.4 (Ar-C), 125.7 (Ar-C), 123.0 (Ar-C), 121.0 (Ar-C). HRMS (ESI) m/z: calculated for $C_{17}H_{11}BrO_4S$ $[M+H]^+$: 390.9600; found: 390.96295.

Anal. Cald. For $C_{17}H_{11}BrO_4S$: C, 52.19; H, 2.83; S, 8.20; Found: C, 52.39; H, 2.95; S, 7.89.

2.2.4. 1-Formylnaphthalen-2-yl 2,5-dichlorobenzenesulfonate (3d)

Light cream powder (benzene-hexane (1:5)); m.p 154–156 °C; mol. wt: 379.97; yield 51%. FT-IR (pure, cm^{-1}) ν: 3089.28 (sp^2 C-H), 1685.30 (ArHC = O), 1574.23, 1509.32 (Ar C-C), 1381.63 ($ArSO_2OAr$), 1168.16, ($ArSO_2OAr$). ^1H NMR(400 MHz, $CDCl_3$), δ/ppm: 10.70 (s, 1H, CHO), 9.21 (d, 1H, $J = 8.70$ Hz, Ar-H), 8.09 (d, 1H, $J = 9.00$ Hz, Ar-H), 8.02 (s, 1H, Ar-H), 7.90 (d, 1H, $J = 8.10$ Hz, Ar-H), 7.76–7.69 (dd, 1H, $J = 11.40$, 4.10 Hz, Ar-H), 7.67–7.58 (m, 3H, Ar-H), 7.38 (d, 1H, $J = 9.00$ Hz, Ar-H). ^{13}C NMR (100 MHz,$CDCl_3$), δ/ppm: 190.1 (Ar-CHO), 152.4 (Ar-C), 136.7 (Ar-C), 135.7 (Ar-C), 134.5 (Ar-C), 133.7 (Ar-C), 133.6 (Ar-C), 132.2 (Ar-C), 131.9 (Ar-C), 131.7 (Ar-C), 130.7 (Ar-C), 130.1 (Ar-C), 128.4 (Ar-C), 127.4 (Ar-C), 125.8 (Ar-C), 123.2 (Ar-C), 120.5 (Ar-C). HRMS (ESI) m/z: calculated for $C_{17}H_{10}Cl_2O_4S$ $[M + H]^+$: 380.9700; found: 380.97446. Anal. Cald. For $C_{17}H_{10}Cl_2O_4S$: C, 53.56; H, 2.64; S, 8.41; Found: C, 53.31; H, 2.64; S, 8.25.

2.2.5. 1-Formylnaphthalen-2-yl 2,4,6-triisopropylbenzenesulfonate (3e)

Light cream powder (benzene-hexane (1:5)); m.p 139–141 °C; mol. wt: 460.18; yield 53%. FT-IR (KBr, cm^{-1}) ν: 2971.42, 2956.67, 2925.00(sp^2 C-H), 2885.71, 2867.85 (sp^3 C-H), 1688.48 (ArHC = O), 1597.30, 1508.91 (Ar C-C), 1350.76 ($ArSO_2OAr$), 1169.40, ($ArSO_2OAr$). ^{1}HNMR (400 MHz, $CDCl_3$), δ/ppm: 10.70 (s, 1H, CHO), 9.27 (d, 1H, $J = 8.70$ Hz, Ar-H), 8.02 (d, 1H, $J = 8.90$ Hz, Ar-H), 7.86 (d, 1H, $J = 8.10$ Hz, Ar-H), 7.71 (t, 1H, $J = 7.80$ Hz, Ar-H), 7.59 (t, 1H, $J = 7.5$ Hz, Ar-H), 7.28 (s, 2H, Ar-H), 7.12 (d, 1H, $J = 8.90$ Hz, Ar-H), 4.13–3.97 (m, 2H, 2 units of Ar-$CH(CH_3)_2$), 3.05–2.93 (m, 1H, 1 unit of Ar-$CH(CH_3)_2$), 1.32 (d, 6H, $J = 6.90$ Hz, 1 unit of Ar-$CH(CH_3)_2$), 1.23(d, 12H, $J = 6.7$ Hz, 2 units of Ar-$CH(CH_3)_2$). ^{13}C NMR (100 MHz, $CDCl_3$), δ/ppm: 190.7 (Ar-CHO), 155.0 (Ar-C), 153.5 (Ar-C), 151.2 (Ar-C), 136.4 (Ar-C), 132.0 (Ar-C), 130.9 (Ar-C), 129.9 (Ar-C), 129.6 (Ar-C), 128.2 (Ar-C), 127.0 (Ar-C), 125.8 (Ar-C), 124.3 (2 units of Ar-C), 123.4 (Ar-C), 120.6 (2 units of Ar-C), 34.3 (1 unit of Ar-$CHCH_3$), 30.0 (1 signal for 2 units of Ar-$CHCH_3$), 24.6 (1 signal for 2 units of Ar-$CH(CH_3)_2$), 23.5 (1 signal for 1 unit of Ar-$CH(CH_3)_2$). HRMS (ESI) m/z: calculated for $C_{26}H_{30}O_4S$ $[M + Na]^+$: 461.1800; found: 461.17430. Anal. Cald. For $C_{26}H_{30}O_4S$: C, 71.20; H, 6.89; S, 7.31; Found: C, 71.75; H, 7.37; S, 7.22.

2.2.6. 1-Formylnaphthalen-2-yl naphthalene-2-sulfonate (3f)

Light cream powder (benzene-hexane (1:5)); m.p 140–142 °C; mol. wt: 362.06; yield 71%. FT-IR (KBr, cm^{-1}) ν:3053.57 (sp^2 C-H), 1688.87 (ArHC = O), 1587.51, 1509.09 (Ar C-C), 1376.99 ($ArSO_2OAr$), 1173.45 ($ArSO_2OAr$). ^1H NMR (400 MHz, DMSO-d6) δ/ppm: 10.40(s, 1H, CHO), 8.93 (d, 1H, $J = 8.70$ Hz, Ar-H), 8.65 (s, 1H, Ar-H), 8.27–8.17 (m, 3H, Ar-H), 8.11 (d, 1H, $J = 8.20$ Hz, Ar-H), 8.01 (d, 1H, $J = 8.10$ Hz, Ar-H), 7.91 (dd, 1H, $J = 8.7$ Hz, 2.0 Hz, Ar-H), 7.81–7.76 (m, 1H, Ar-H), 7.73–7.67 (m, 2H, Ar-H), 7.64–7.59 (m, 1H, Ar-H), 7.26 (d, 1H, $J = 9.00$ Hz, Ar-H). ^{13}C NMR (100 MHz, DMSO-d6), δ/ppm: 190.2 (Ar-CHO), 152.4 (Ar-C),137.4 (Ar-C),135.7(Ar-C),132.2(Ar-C),131.9(Ar-C),131.3(Ar-C),130.8(Ar-C),130.8 (Ar-C), 130.7 (Ar-C), 130.4 (Ar-C), 130.3 (Ar-C), 130.2 (Ar-C), 129.2 (Ar-C), 128.6 (Ar-C), 128.5 (Ar-C), 127.7 (Ar-C), 125.1 (Ar-C), 123.2 (Ar-C), 122.8 (Ar-C), 121.7 (Ar-C). HRMS (ESI) m/z: calculated for $C_{21}H_{14}O_4S$ $[M + H]^+$: 363.0600, found: 363.0600. Anal. Cald. For $C_{21}H_{14}O_4S$: C, 69.60; H, 3.89; S, 8.85; Found: C, 69.39; H, 3.84; S, 8.73.

2.2.7. Naphthalen-2-yl 4-fluorobenzenesulfonate (3 g)

Dark cream powder (benzene-hexane (1:5)); m.p 84–86 °C; mol. wt: 302.03; yield 66%. FT-IR (KBr, cm^{-1}) ν: 2953.95 (sp^2 C-H), 1598.94, 1508.40 (Ar C-C), 1378.11 ($ArSO_2OAr$), 1181.48, ($ArSO_2OAr$). ^1H NMR (400 MHz, $CDCl_3$), δ/ppm: 7.91–7.83 (m, 3H, Ar-H), 7.81–7.75 (m, 2H, Ar-H), 7.55–7.50 (m, 2H, Ar-H), 7.49–7.48 (m, 1H, Ar-H), 7.25–7.18 (m, 2H, Ar-H), 7.15–7.09 (m, 1H, Ar-H). ^{13}C NMR (100 MHz, $CDCl_3$), δ/ppm: 167.4 (Ar-C), 164.7 (Ar-C), 147.0 (Ar-C), 133.4 (Ar-C), 131.9 (Ar-C), 131.5 (Ar-C), 131.4 (Ar-C), 129.9 (Ar-C), 127.9 (Ar-C), 127.8 (Ar-C), 127.0 (Ar-C), 126.5 (Ar-C), 120.9 (Ar-C), 119.9 (Ar-C), 116.7 (Ar-C), 116.4 (Ar-C). HRMS (ESI) m/z: calculated for $C_{16}H_{11}FO_3S$ $[M + Na]^+$: 325.0300; found: 325.0301. Anal. Cald. For $C_{16}H_{11}FO_3S$: C, 63.57; H, 3.67; S, 10.61; Found: C, 63.49; H, 3.45; S, 10.25.

2.2.8. Naphthalen-2-yl 2,5-dichlorobenzenesulfonate (3 h)

Light cream powder (benzene-hexane (1:5)); m.p 108–109 °C; mol. wt: 351.96; yield 65%. FT-IR (KBr, cm^{-1}) ν: 3092.85, 3067.85(sp^2 C-H), 1507.73, 1447.78 (Ar C-C), 1351.64 ($ArSO_2OAr$), 1185.85, ($ArSO_2OAr$). ^1H NMR (400 MHz, $CDCl_3$), δ/ppm: 7.95 (m, 1H, Ar-H), 7.89–7.78 (m, 3H, Ar-H), 7.65 (s, 1H, Ar-H), 7.62–7.50 (m, 4H, Ar-H), 7.34–7.26 (m, 1H, Ar-H). ^{13}C NMR (100 MHz, $CDCl_3$), δ/ppm: 146.7 (Ar-C), 135.1 (Ar-C), 134.9 (Ar-C), 133.44 (Ar-C), 133.40 (Ar-C), 133.2 (Ar-C), 132.1 (Ar-C), 131.5 (Ar-C), 130.2 (Ar-C), 128.3 (Ar-C), 127.9 (Ar-C), 127.8 (Ar-C), 127.1 (Ar-C), 126.6 (Ar-C), 120.4 (Ar-C), 119.6 (Ar-C). HRMS (ESI) m/z: calculated for $C_{16}H_{10}Cl_2O_3S$ $[M + Na]^+$: 374.9600; found: 374.9623. Anal. Cald. For $C_{16}H_{10}Cl_2O_3S$: C, 54.41; H, 2.85; S, 9.08; Found: C, 54.12; H, 3.13; S, 8.77.

2.2.9. Naphthalen-2-yl 2,4,6-trimethylbenzenesulfonate (3i)

Light cream powder (benzene-hexane (1:5)); m.p 154–155 °C; mol. wt: 326.10; yield 52%. FT-IR (KBr, cm^{-1}) ν: 3060.71(sp^2 C-H), 2971.42, 2932.14 (sp^3 C-H) 1597.50, 1508.22, 1457.99 (Ar C-C), 1364.30 ($ArSO_2OAr$), 1191.14($ArSO_2OAr$). ^1H NMR (400 MHz, $CDCl_3$), δ/ppm: 7.85–7.73 (m, 3H, Ar-H), 7.55–7.43 (m, 3H, Ar-H), 7.13 (d, 1H, $J = 8.90$ Hz, Ar-H), 6.99 (s, 2H, Ar-H), 2.60 (s, 6H, 2 units of Ar-CH_3), 2.34 (s, 3H, Ar-CH_3); ^{13}C NMR (100 MHz, $CDCl_3$), δ/ppm: 147.0 (Ar-C), 143.8 (Ar-C), 140.5 (Ar-C), 133.5 (Ar-C), 133.4 (Ar-C), 131.8 (1 signal for 2 units of Ar-C), 130.6 (Ar-C), 129.7 (1 signal for 2 units of Ar-C), 127.8 (Ar-C), 127.7 (Ar-C), 126.8 (Ar-C), 126.3 (Ar-C), 122.8 (1 signal for 2 units of Ar-CH_3), 121.1 (Ar-CH_3), 121.0 (Ar-C), 119.7 (Ar-C). HRMS (ESI) m/z: calculated for $C_{19}H_{18}O_3S$ $[M + H]^+$:

326.1000; found: 326.10495. Anal. Cald. For $C_{19}H_{18}O_3S$: C, 69.91; H, 5.56; S, 9.82; Found: C, 69.39; H, 6.17; S, 9.51.

2.2.10. Naphthalen-2-yl 2,4,6-triisopropylbenzenesulfonate (3j)

Light cream powder (benzene-hexane (1:5)); m.p 70–72 °C; mol. wt: 432.18; yield 51%. FT-IR (KBr, cm^{-1}) ν: 3035.71(sp^2 C-H), 2967.85, 2953.85, 2925.00, 2867.85 (sp^3 C-H) 1599.24, 1508.09, 1458.20 (Ar C-C), 1378.22 ($ArSO_2OAr$), 1181.17($ArSO_2OAr$). ^{1}H NMR (400 MHz, $CDCl_3$), δ/ppm: 7.85–7.78 (m, 2H, Ar-H), 7.76–7.69 (m, 1H, Ar-H), 7.53–7.46 (m, 3H, Ar-H), 7.39 (s, 1H, Ar-H), 7.24 (s, 1H, Ar-H), 7.22–7.16 (m, 1H, Ar-H), 4.22–4.08 (m, 2H, 2 units of Ar-$CH(CH_3)_2$), 3.05–2.93 (m, 1H, 1 unit of Ar-$CH(CH_3)_2$), 1.31 (m, 6H, 1 unit of Ar-$CH(CH_3)_2$), 1.20 (m, 12H, 2 units of Ar-$CH(CH_3)_2$). ^{13}C NMR (100 MHz, $CDCl_3$), δ/ppm: 154.3 (Ar-C), 151.2 (Ar-C), 147.1 (Ar-C), 133.4 (Ar-C), 131.8 (Ar-C), 129.9 (Ar-C), 129.77 (Ar-C), 127.72 (Ar-C), 126.8 (Ar-C), 126.2 (Ar-C), 123.9 (2 units of Ar-C), 121.3 (Ar-C), 119.7 (2 units of Ar-C), 34.2 (1 unit of Ar-$CHCH_3$), 29.8 (1 signal for 2 units of Ar-$CHCH_3$), 24.5 (1 signal for 2 units of Ar-$CH(CH_3)_2$), 23.5 (1 signal for 1 unit of Ar-$CH(CH_3)_2$). HRMS (ESI) m/z: calculated for $C_{25}H_{30}O_3S$ $[M+H]^+$: 433.1800; found 433.1811. Anal. Cald. For $C_{25}H_{30}O_3S$: C, 73.13; H, 7.36; S, 7.81; Found: C, 73.71; H, 7.48; S, 7.46.

2.3. In vitro tyrosinase inhibition assay

Tyrosinase inhibition properties of the screened naphthalene compounds were determined according to a previous study (Korkmaz & Bursal, 2022b). Briefly, different concentrations (20–160 μM) of the screened compounds in 130 μL phosphate buffer (0.05 M, pH 6.8) and 50 μL tyrosine substrate solutions were pipetted to a 96-well microplate. The reaction was started by adding 25 μL (25 EU) mushroom tyrosinase enzyme solution. After the incubation of 5 min period at 25 °C, the microplate was run in the spectrophotometer at 490 nm and the absorbance changes for 5 min were recorded. Also, the control sample (the same procedure only without adding the tested compounds was used to compare the results of the samples. The following equation was used to calculate the inhibitions of compounds against tyrosinase and pancreatic lipase activities.

$$\%inhibition = \frac{A-B}{A} \times 100$$

In this equation ***A*** is the absorbance of the control sample and ***B*** is the absorbance of the screened samples. The compounds' IC_{50} values (concentration of a compound able to inhibit 50% of the enzyme activity) were calculated from the obtained equations of the activity-concentration graph.

2.4. In vitro pancreatic lipase inhibition assay

Enzyme inhibition properties of the screened **3a-j** compounds against pancreatic lipase (PL) were determined according to a previous study (Korkmaz & Bursal, 2022c). Firstly, the PL solution was prepared by solving 100 mg porcine pancreatic lipase in a 10 mL buffer solution (0.05 M, pH: 6.8) and centrifuged for 10 min (4000 rpm). The supernatant was separated and stored as PL enzyme stock solution for the enzyme assays. The different concentrations of compounds (20–160 μM) in the buffer solution and 20 μL of enzyme solution were pipetted to a 96-well microplate and incubated for 5 min at 37 °C. Then, 20 μL of the substrate (4-nitrophenyl butyrate, 10 mM in acetonitrile) was added to each microplate well. The microplate was run in a spectrophotometer (Thermo Scientific Multiskan GO) at 405 nm. Orlistat was used as a positive standard in the procedure.

2.5. Quantum chemical calculations

Three-dimensional (3 D) structures of pancreatic lipase and tyrosinase inhibitor candidates were prepared with GaussView 5.0 (Dennington et al., 2009) and the geometry optimization studies were performed by using Gaussian 09 program suite (Frisch et al., 2016) at the DFT/B3LYP/6-311g(d,p)) level of theory. In the concomitant step, the optimized structures were checked to be accurate relative energy minima of the potential energy surfaces through corresponding frequency calculations, and no imaginary frequencies indicate the intrinsic stability of the investigated compounds. The details of these calculations are provided in ESI†.

2.6. Molecular docking analysis

Molecular docking studies were performed using the previously reported protocol (Korkmaz et al., 2022). UCSF Chimera, AutoDock Vina, ChemDraw Ultra 12.0, Avogadro, Biovia Discovery Studio Visualizer, and PyMOL visualization software were employed (Biovia, 2017; Hanwell et al., 2012; Pettersen et al., 2004; Schrödinger LLC, 2021; Trott & Olson, 2010). The binding pocket coordinates of the compounds were employed for tyrosinase (center x,y,z: −7.59, 46.56, 84.98, size x,y,z: 11, 11, 11) and pancreatic lipase (center x,y,z: 54.73, 46.87, 122.10, size x,y,z: 14, 14, 14). PyMOL visualization software was used to prepare superimposing images (Schrödinger LLC, 2021). The interactions of structures were envisioned using Biovia Discovery Studio Visualizer (Biovia, 2017).

2.7. PreADMET studies

ADME, drug-likeness, physicochemical properties, and toxicity prediction of the naphthalene derivatives bearing functional sulfonates were performed by PreADMET and Molinspiration software (Lee et al., 2017; Molinspiration, 2011).

3. Results and discussion

3.1. Synthesis

In this study, a subgroup of sulfonate derivatives possessing naphthalene scaffold on their structural motifs was modeled to distinguish their structural and biological properties. Their backbones were decorated with aryl substituents; namely 4-chlorophenyl, 2-naphthyl, 4-fluorophenyl, 2,5-dichlorophenyl, 4-methoxyphenyl, 2,4,6-trimethylphenyl, 2,4,6-triisopropylphenyl,

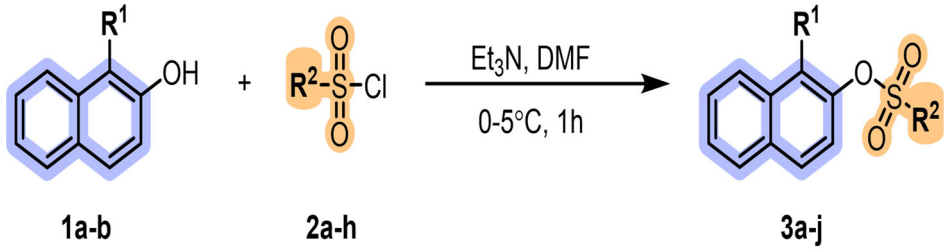

Entry	R^1	R^2	Entry	R^1	R^2
3a	-CHO	4-$MeOC_6H_4$	3f	-CHO	$C_{10}H_7$
3b	-CHO	4-ClC_6H_4	3g	-H	4-FC_6H_4
3c	-CHO	4-BrC_6H_4	3h	-H	2,5-$(Cl)_2C_6H_3$
3d	-CHO	2,5-$(Cl)_2C_6H_3$	3i	-H	2,4,6-$(CH_3)_3C_6H_2$
3e	-CHO	2,4,6-$((CH_3)_2CH)_3C_6H_2$	3j	-H	2,4,6-$((CH_3)_2CH)_3C_6H_2$

Scheme 2. TEA-mediated facile synthesis of naphthalene-bearing sulfonate derivatives.

and 4-bromophenyl. During the wet-lab studies, the target molecules were prepared by implementing a similar synthetic protocol (Korkmaz & Bursal, 2022b).The naphthalene-based sulfonate derivatives were obtained at a 1.2 TEA-Base/substrate ratio, in 1 hour, and reactions were conducted at 0–5 °C (Scheme 2).

With the completion of the optimization studies, based on this determined one-step reaction pathway, we could obtain the target sulfonate derivatives **3a-j** in good yields.

3.2. Structural characterization

The naphthalene-based sulfonate derivatives were purified, and structural characterization of the compounds **3a-j** was accomplished using appropriate techniques, including FT-IR, ^{1}H-NMR, ^{13}C-NMR, HRMS, and elemental analysis.

The FT-IR spectra for a typical aldehyde carbonyl peak of **3a, 3 b, 3c, 3d, 3e,** and **3f** were observed at 1686.95, 1685.73, 1685.67, 1685.30, 1688.48, and 1688.87 cm^{-1}, respectively, while the rest of compounds **3 g, 3 h, 3i**, and **3j** did not appear at this region. In addition, the observation of specific strong $ArSO_2OAr$ band peaks (approximately 1380 and 1180 cm^{-1}) in the FT-IR spectra of all compounds **3a-j** indicated that the compounds were bound with aryl sulfonyl chlorides.

The naphthalene-based sulfonate derivatives **3a-f** exhibited the aldehyde (Ar-C**H**O) protons as characteristic singlets at 10.42, 10.34, 10.47, 10.70, 10.70, and 10.40 ppm, respectively. Also, the absence of -OH peaks of compounds **3a-j** in the ^{1}H NMR spectrum has indicated the bonding formation of the sulfonate structures.

The formyl peak of **3a** among the compounds with the best efficacy was consistent at 10.42 ppm in the 1H NMR spectrum.**3a** has demonstrated two multiplets centered from 7.70 to 7.64 ppm as one proton and 7.62–7.56 ppm as one proton. In addition, six doublet signals of **3a** were observed at 9.16 (d, 1H, $J = 8.60$ Hz, Ar-H), 8.07 (d, 1H, $J = 9.00$ Hz, Ar-H), 7.88 (d, 1H, $J = 8.10$ Hz, Ar-H), 7.77 (d, 2H, $J = 8.90$ Hz, Ar-H), 7.36 (d, 1H, $J = 9.00$ Hz, Ar-H), and 6.99 (d, 2H, $J = 8.90$ Hz, Ar-H) due to the benzene and naphthyl moiety. Also, the methoxy proton peak of **3a** was observed as a single signal at 3.90 ppm. Consequently, the number of protons observed in this compound is consistent with the expected number of protons in the ^{1}H NMR spectrum. The synthesized sulfonate derivatives bearing different substituents **3a-j** are depicted in Table 1.

Similarly, the proton signals of **3i** due to the aromatic moiety were monitored at 7.85–7.73 (m, 3H, Ar-H), 7.55–7.43 (m, 3H, Ar-H), 7.13 (d, 1H, $J = 8.90$ Hz, Ar-H), and 6.99 (s, 2H, Ar-H) in the aromatic region. Three methyl signals (two methyl peaks overlapped) of **3i** were observed at two signals at 2.60 and 2.34 ppm as singlets in the aliphatic region. In other compounds, the proton peaks were compatible as expected (see supplemental data).

All ^{13}C NMR signals of compounds **3a-j** were clearly determined (see supplemental data). The expected formyl carbon peaks of six compounds **3a-f** were measured at 189.9, 190.0, 189.6, 190.1, 190.7, and 190.2 ppm, respectively. As expected, no formyl peak was observed in other compounds **3 g, 3 h, 3i,** and **3j**. As expected, 16 carbon peaks in ^{13}C NMR of the compounds **3a, 3 b, 3c, 3e, 3i,** and **3j** were observed in the aromatic region 14 carbon signals which are two of these peaks overlapped the two co-peaks. The carbon peaks of compounds **3d, 3f, 3 g,** and **3 h** were observed as the expected peaks. All of the HRMS masses were predicted as [M + Na] and [M + H] values. The HRMS spectra values of compounds **3a-j** showed the expected molecular peak of pure compounds. As a result, spectrum analyzes of compounds **3a-j** showed that these compounds were obtained in pure form. All of the CHNS elemental analyses were corrected the compounds.

3.3. Determination of tyrosinase inhibitory activities

The synthesized naphthalene-bearing sulfonate derivatives were screened to see their effects on tyrosinase enzyme activity. The IC_{50} values were calculated to predict their inhibitor potentials. The IC_{50} values of the synthesized

Table 1. Structures of the naphthalene-based sulfonate derivatives **3a-j**.

Compounds	R^1	R^2	Compounds	R^1	R^2
3a	Ar**HC** = **O**	4-$MeOC_6H_4$	**3f**	Ar**HC** = **O**	$C_{10}H_7$
3b	Ar**HC** = **O**	4-ClC_6H_4	**3g**	**H**	4-FC_6H_4
3c	Ar**HC** = **O**	4-BrC_6H_4	**3h**	**H**	2,5-$(Cl)_2C_6H_3$
3d	Ar**HC** = **O**	2,5-$(Cl)_2C_6H_3$	**3i**	**H**	2,4,6-$(CH_3)_3C_6H_2$
3e	Ar**HC** = **O**	2,4,6-$((CH_3)_2CH)_3C_6H_2$	**3j**	**H**	2,4,6-$((CH_3)_2CH)_3C_6H_2$

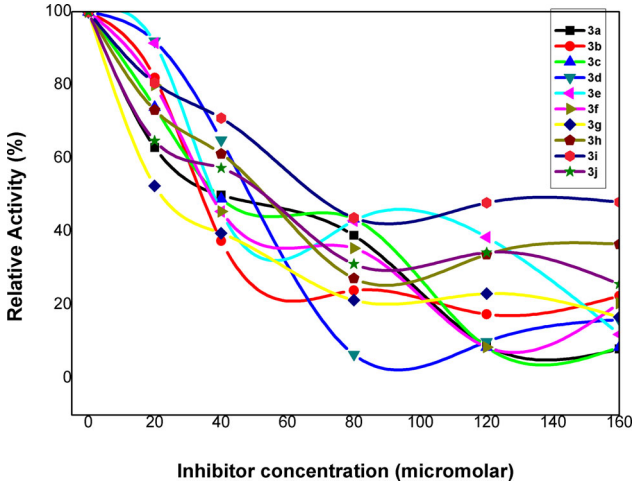

Figure 1. Tyrosinase inhibition effects of the investigated sulfonate derivatives.

compounds were calculated in the range of 40.8 ± 3.34 μM and 112.6 ± 6.7 μM. The enzyme inhibitory activities of the compounds were compared to kojic acid, a well-known tyrosinase inhibitor. Among the synthesized compounds, **3a**, **3c**, and **3d** were determined to have more effective tyrosinase inhibitions. The IC_{50} values of **3a** (40.8 ± 3.3), **3c** (43.3 ± 3.5), and **3d** (43.3 ± 3.6) were determined to be comparable levels to the kojic acid IC_{50} value (19.2 ± 0.3 μM) which was noted in a recent study (Song et al., 2021).Also, the inhibitory activities of the compounds were calculated as kojic acid equivalent (KAEq) to compare their results with the standard inhibitor. The KAEq values of the synthesized compounds were calculated in the range of 0.17 and 0.47 KAEq. The results suggest that all investigated compounds' inhibitory activities were lower than the kojic acid. The inhibition effects of the synthesized compounds on tyrosinase enzyme were given as activity/concentration graph in Figure 1. Herein, the decreasing enzyme activity (%) shows the inhibitor power of the compound.

Tyrosinase catalyzes the hydroxylation of L-tyrosine and the oxidation of L-DOPA (3,4-dihydroxyphenylalanine) to o-dopaquinone. Tyrosinase contains a copper complex in the catalytic center and hydroxyl groups of the substrate are suggested to be bound to the copper atoms causing inhibition of the enzyme. Overall, most of the screened compounds showed moderate inhibition against tyrosinase compared to the standard compound (kojic acid). Generally, the existence of halogen substitutions increased tyrosinase inhibition. In terms of the structure-activity relationship point, the tyrosinase inhibition activity order of the most effective sulfonate derivatives with having different substituents was found to be compounds **3a** (methoxybenzene), **3c** (bromobenzene), and **3d** (dichlorobenzene), respectively.

Various researchers evaluated the tyrosinase inhibitory activities of many synthetic or natural compounds. Inhibition effects of many phenolics, flavonoids, coumarins, chalcones, terpenoid natural compounds and pyridine, carbazone, azole, and thiazolidine derivatives synthetic compounds were collected in a paper as a comprehensive review on tyrosinase inhibitors (Zolghadri et al., 2019).

Structure-activity relationship studies showed that the existence and location of the hydroxyl groups on aromatic rings are the essential factors in the tyrosinase inhibition effects of natural or synthetic compounds. Kojic acid which is as a well-known tyrosinase inhibitor, has two hydroxyl groups in its chemical structure. Although the synthesized sulfonate compounds do not contain hydroxyl groups, their halogen substitutions are considered to affect tyrosinase inhibition. A previous study reported that halogen-substituted sulfonamide derivatives could reduce tyrosinase activity and showed potent tyrosinase inhibitions (Huo et al., 2021).

3.4. Determination of pancreatic lipase inhibitory activities

The inhibition IC_{50} values of the synthesized compounds on pancreatic lipase were calculated to be between the range of 95.3 ± 4.0 μM and 173.2 ± 4.7 μM. All of the compounds **3a-j** were determined to have slightly higher IC_{50} values than the orlistat IC_{50} value (63.0 ± 4.8 μM). Among the synthesized compounds, **3 h** and **3e** were determined to have more effective pancreatic lipase inhibitions than the other compounds. The IC_{50} values of the **3 h** (95.3 ± 4.0 μM) and **3e** (99.0 ± 2.7 μM) were determined to be at comparable levels to the orlistat IC_{50} value. Also, pancreatic lipase inhibitions of the compounds were determined as orlistat equivalent (OEq) to compare their results with the standard inhibitor. The OEq values of the synthesized compounds were calculated between 0.36 and 0.66 OEq. Remarkably, most of the screened compounds showed around half of the inhibitory effect of orlistat (0.5 OEq) (Table 2). According to the data of this study, **3 h** was detected to be the most effective inhibitor against the pancreatic lipase understood from the lowest IC_{50} value (95.3 ± 4.0 μM) and highest orlistat equivalent value (0.66 OEq). The inhibition effects of the synthesized compounds **3a-j** on pancreatic lipase were given as an activity/concentration graph in Figure 2.

Orlistat is approved to be the main drug in the clinical treatment of obesity as a pancreatic lipase inhibitor. Orlistat has both lipophilic and hydrophilic parts in its chemical structure. When we checked the structure-activity relationship of the synthesized compounds with orlistat, the most potent inhibitor substituents have relatively larger lipophilic

Table 2. *In vitro* enzyme inhibition results with IC_{50} and equivalent standard values.

	Tyrosinase inhibition		Pancreatic lipase inhibition	
Compound code	IC_{50} value (μM)	Kojic acid Equivalent (KAEq)	IC_{50} value (μM)	Orlistat equivalent (OEq)
3a	**40.8 ± 3.3**	**0.47**	115.5 ± 3.2	0.55
3b	57.8 ± 4.6	0.33	115.5 ± 5.7	0.55
3c	**43.3 ± 3.5**	**0.44**	173.3 ± 4.7	0.36
3d	**43.3 ± 3.6**	**0.44**	173.3 ± 4.6	0.36
3e	63.0 ± 5.0	0.30	**99.0 ± 2.7**	**0.64**
3f	49.5 ± 3.9	0.39	138.6 ± 3.8	0.45
3g	99.0 ± 1.0	0.19	131.0 ± 8.9	0.48
3h	112.6 ± 6.7	0.17	**95.3 ± 4.0**	**0.66**
3i	55.6 ± 3.2	0.35	118.5 ± 11.0	0.53
3j	53.6 ± 5.8	0.36	100.5 ± 8.9	0.63
Kojic acid[a]	19.2 ± 0.3	1.0		
Orlistat[b]			63.0 ± 4.8	1.0

The bond highlighted values are the low IC_{50} values which show the effective inhibition.
[a]Standard inhibitor of tyrosinase.
[b]Standard inhibitor of pancreatic lipase.

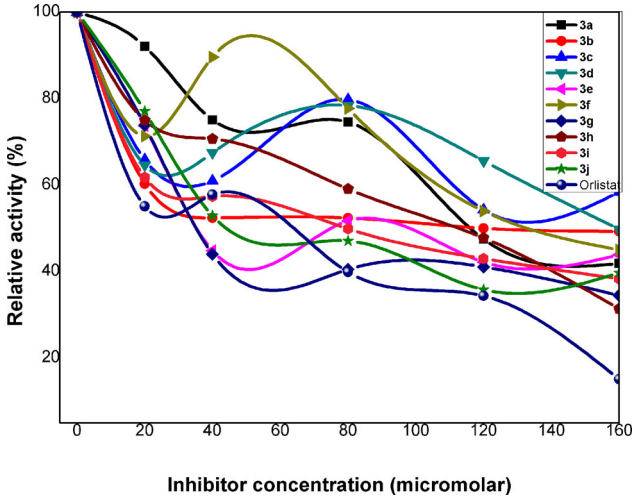

Figure 2. Pancreatic lipase inhibition effects of the investigated sulfonate derivatives **3a-j**.

Table 3. Calculated frontier orbital energies and global reactivity descriptors [B3LYP/6-311G(d,p)].

Entry	ε_{HOMO}[1]	ε_{LUMO}[a]	εgap[b]	I[c]	A[c]	μ[d]
3a	−6.547	−2.346	4.201	6.547	2.346	6.947
3b	−6.712	−2.524	4.188	6.712	2.524	6.126
3c	−6.705	−2.524	4.181	6.705	2.524	6.099
3d	−6.692	−2.499	4.193	6.692	2.499	4.630
3e	−6.437	−2.220	4.217	6.437	2.220	6.710
3f	−6.567	−2.405	4.162	6.567	2.405	7.105
3g	−6.371	−1.777	4.594	6.371	1.777	4.628
3h	−6.422	−2.116	4.305	6.422	2.116	5.353
3i	−6.268	−1.604	4.664	6.268	1.604	5.542
3j	−6.279	−1.593	4.686	6.279	1.593	5.269

[a]in eV. [b]bandgap energy calculated from ε_{LUMO}-ε_{HOMO} (in eV). [c]global reactivity descriptors (I: ionization potential calculated from -ε_{HOMO} (in eV), A: electron affinity calculated from -ε_{LUMO} (in eV). [d]dipole moment (in Debye).

parts than the others. In terms of the structure-activity relationship point, the pancreatic lipase inhibition activity order of the synthesized sulfonate derivatives with having different substituents was found to be standard compound (**orlistat**) > **3 h** (naphthalen-2-yl 2,5-dichlorobenzenesulfonate) > **3e** (1-formylnaphthalen-2-yl 2,4,6-triisopropylbenzenesulfonate) > **3j** (naphthalen-2-yl 2,4,6-triisopropylbenzenesulfonate), respectively. According to the results, the existence of halogen and triisopropyl substitutions causes pancreatic lipase inhibition.

In recent years, some studies have evaluated the inhibition potentials of various sulfonate compounds against some enzymes. Analyses of naphthalene-bearing sulfonate compounds provide insights into the relationship between the pancreatic lipase inhibitory effects and substituted naphthalene groups. The compound **3 h**, which contains naphthalen-2-yl 2,5-dichlorobenzene substitution, was detected to be the most effective inhibitor of pancreatic lipase. Likewise, a former study reported that 2-naphthyl unit moiety was beneficial for pyrazolone derivatives to inhibit the pancreatic lipase enzyme (Zhang et al., 2021).

Overall, the synthesized naphthalene-bearing sulfonate derivatives showed diverse effects on tyrosinase and pancreatic lipase enzymes. According to the gathered results, **3 h** demonstrated the most effective inhibition against pancreatic lipase, whereas **3a** was the most effective inhibitor against tyrosinase. Remarkably, they had opposite effects on the enzymes due to the active sites of the enzymes. For instance, **3 h** and **3e** were detected to be the most effective inhibition against pancreatic lipase, but their tyrosinase inhibitions were at low values compared to the standards.

3.5. Quantum chemical calculations

As already stated, we intended to contribute a viable strategy to improve the inhibitor activity of sulfonate derivatives against pancreatic lipase and tyrosinase. Thus, we decided to retain the identical naphthalene subunits on the backbone of the target compounds, whereas we decorated them with divergent subunits. Therefore, a systematic approach to evaluate the physicochemical behaviors of the investigated molecules is to perform first experimentally. Then, the DFT calculations were followed by enzyme activity and molecular docking studies. At first glance, to preliminarily appraise the potent activity of the mentioned naphthalene possessing sulfonate derivatives, we have computationally investigated target compounds by performing geometry optimization and subsequently executed frequency calculations to ensure their local minima. According to the obtained data, we have predicted frontier orbital energies comprising HOMO (Highest Occupied Molecular Orbital, LUMO (Lowest Unoccupied

Table 4. Frontier molecular orbital's contour plots, Mulliken charge distribution, dipole moment vector, and ESP maps for the most effective tyrosinase (**3a**, **3c,** and **3d**) inhibitors among the investigated compounds' series.

Entry	HOMO	LUMO	Mulliken Charges and Dipole Moment (μ) Vector	ESP
3(a)	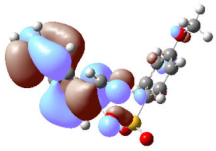	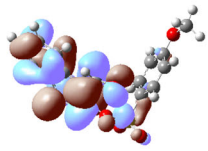	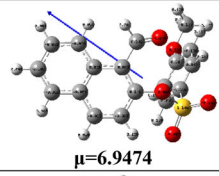 μ=6.9474	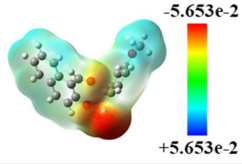 -5.653e-2 +5.653e-2
3(c)	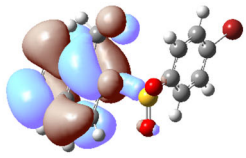	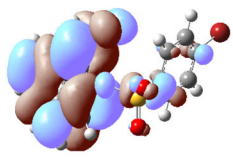	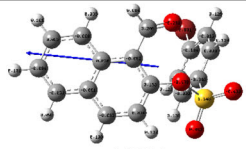 μ=6.0994	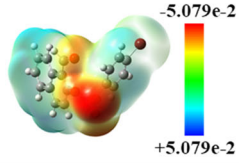 -5.079e-2 +5.079e-2
3(d)	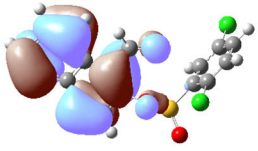	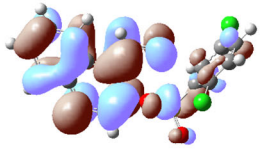	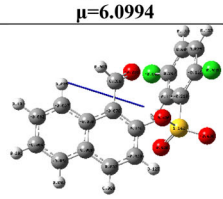 μ=4.6296	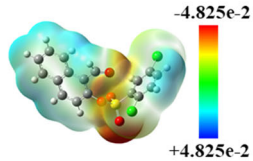 -4.825e-2 +4.825e-2

Table 5. Frontier molecular orbital's contour plots, Mulliken charge distribution, dipole moment vector, and ESP maps for the most effective pancreatic lipase (**3e, 3 h**, and **3j**) inhibitors among the investigated compounds' series.

Entry	HOMO	LUMO	Mulliken Charges and Dipole Moment (μ) Vector	ESP
3(e)	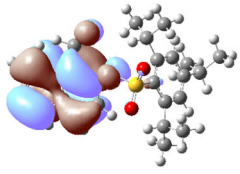	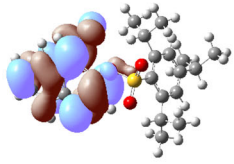	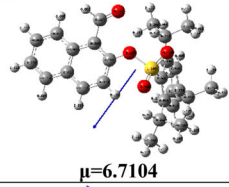 μ=6.7104	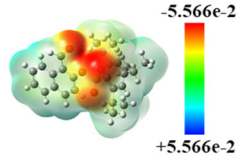 -5.566e-2 +5.566e-2
3(h)	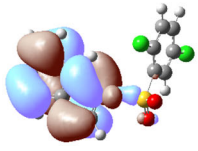	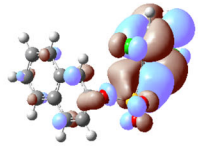	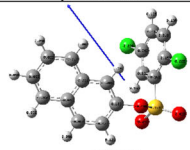 μ=5.3529	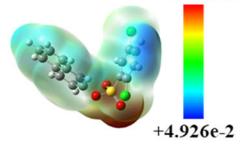 -4.926e-2 +4.926e-2
3(j)	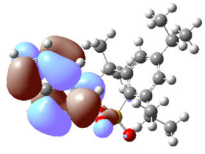	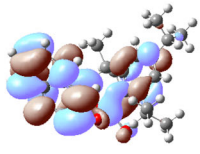	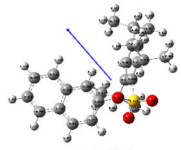 μ=5.2686	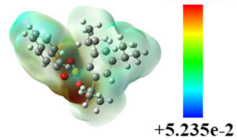 -5.235e-2 +5.235e-2

Molecular Orbital), and relatively their bandgap energies. We have also calculated ionization energies and electron affinity values in the following step. These outputs, including the dipole moment values, are depicted in Table 3.

According to theoretical outputs, it could be depicted that formyl (-CHO) fragment containing molecules (compounds: **3a** to **3f**-included-have unquestionably the lowest bandgap values ranging between 4.162 eV (compound no: **3f**) and 4.217 eV (compound no: **3e**). On the other hand, pristine naphthalene units possessing structures' (compounds **3 g** to **3j**) bandgap energies were found to be between 4.305–4.686 eV. This phenomenon might be explained by the inclusion of the electron-withdrawing groups and their lowering effect on the LUMO energy levels of the target compounds, consequently dominating and reducing the predicted bandgap energy values. In this concept, LUMO energy levels of compounds **3a** to **3f** were found between −2.220 and −2.524 eV, whereas a higher energy distribution pattern was seen as −1.593 to −2.116 eV for the compounds **3 g** to **3j**. As a result, these observations were interpreted in

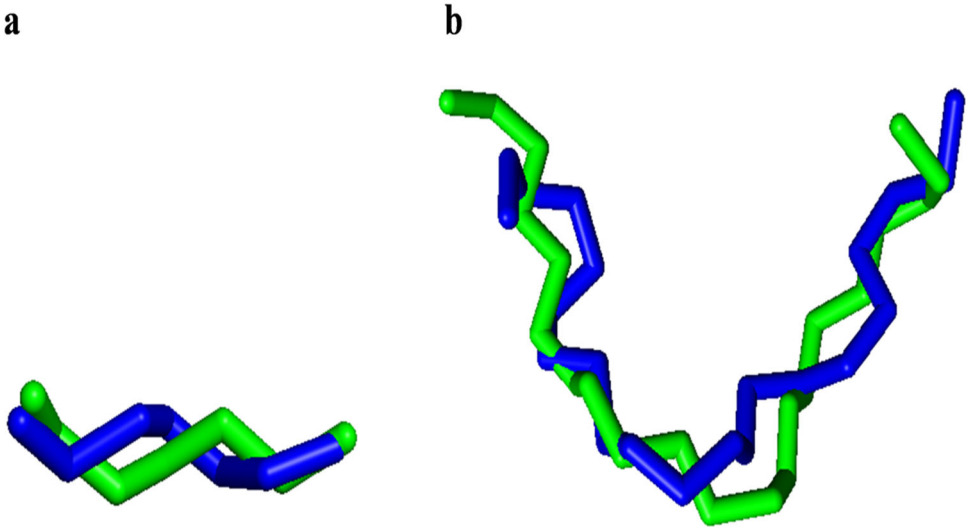

Figure 3. The predicted (blue) and co-crystallized (green) binding modes of the PEG (**a**) and TGME (**b**) for the superimposition poses.

light of the lower bandgap values seen in systems containing formyl units. Following the calculation of the frontier orbital energy values, the representative contour plots of HOMO and LUMO orbitals, Mulliken charge distribution, and electrostatic potential (ESP) maps of the most potent inhibitor candidates for tyrosinase (**3a**, **3c,** and **3d**) and pancreatic lipase (**3e**, **3 h**, and **3j** determined from the enzyme activity studies are also provided in Tables 4 and 5, respectively (also see ESI† for data on the rest of the compounds). Accordingly, HOMO orbitals were predominantly localized on the naphthalene-containing fragment (which acts as a donor unit) for the entire set of investigated compounds. In contrast, LUMO orbitals were mainly localized on the substituent-containing (alkyl, aryl, or haloaryl) subunit part. These two fragments were separated by a sulfonate unit (which could be evaluated as a linker) and resulted in constructing the V-shaped geometrical orientation (corresponding bond angle values varied between 101 and 104°).

Moreover, the corresponding ESP maps revealed the accumulation of the negative electrostatic potential on the sulfonate unit and dominated the rotation of the dipole moment vector. This uniform charge distribution could contribute to the observed enzyme inhibition potential of the investigated molecules against pancreatic lipase and tyrosinase by producing strong electrostatic interactions, including hydrogen bonding and π-π stacking (Pettersen et al., 2004; Trott & Olson, 2010).

3.6. Molecular docking studies

Molecular docking is a required field of study for elucidating protein-ligand interactions. (Alanazi et al., 2022; Aziz et al., 2020, 2021; Elkady et al., 2022). Initially, molecular docking studies were performed for tyrosinase (PDB ID: 2Y9W) with compounds **3a**, **3c**, **3d**, and **3f,** which were the most effective in *in vitro* studies. Also, molecular docking of compounds **3a**, **3e**, **3 h**, and **3j** with pancreatic lipase receptor (PDB ID: 1ETH) was also implemented. The best predicted experimental binding pose and crystallized ligand determined were checked against structural alignment to validate the insertion procedure. It was calculated redocking for the co-crystallized form of di(hydroxyethyl)ether) (PEG) and tetraethylene glycol monooctyl ether (TGME). Root Mean Square Deviations (RMSD) values were found at 0.810 Å (TGME) and 1.608 Å (PEG). The RMSD values are acceptable for validation studies (Menteşe et al., 2018; Mirzazadeh et al., 2021; Yuriev et al., 2011). It exhibited superimposes of the predicted and the co-crystal (Figure 3).

3.6.1. Molecular docking analysis of tyrosinase

The most effective naphthalene-based sulfonate derivatives obtained from the *in vitro* enzyme methods were subjected to molecular docking analyses. For this purpose, compounds **3a**, **3c**, **3d**, and **3f** were used to evaluate *in silico* inhibition activity with tyrosinase (PDB ID: 2Y9W) which was obtained from the Protein Data Bank (PDB) (www.pdb.org). The best affinity of compounds **3a**, **3c**, **3d**, and **3f** with tyrosinase exhibited −8.0, −8.5, −8.3, and −8.7 kcal/mol energy values, respectively (Table 7). The most effective affinity value versus tyrosinase was obtained from **3f** (−8.7 kcal/mol). The 2 D structures and H-bond interaction pose of the naphthalene-based sulfonate derivatives (**3a**, **3c**, **3d**, and **3f)** with tyrosinase were exhibited in Figure 4.

Using the molecular docking study methodology, the best affinity values of kojic acid with tyrosinase were observed as −5.1 kcal/mol. The synthesized compounds (**3a**, **3c**, **3d**, and **3f**) had relative levels with the kojic acid affinity value (Table 6). The interaction of compound **3a** with tyrosinase was determined by a carbon-hydrogen bond (TYR A:310) and conventional hydrogen bond (ASP A:311) as hydrogen bond effects. In addition, it was indicated that Pi-Cation interaction (LYS A:378) and GLU A:355 of the π-anion interaction were noted as an electrostatic effect, as well as PHE A:367 of the π-π T-shaped and LYS A:378 of the π-alkyl interactions were observed as hydrophobic effects. The molecular docking interaction study of compound **3f** with tyrosinase was noted to be the same as with compound **3a**.

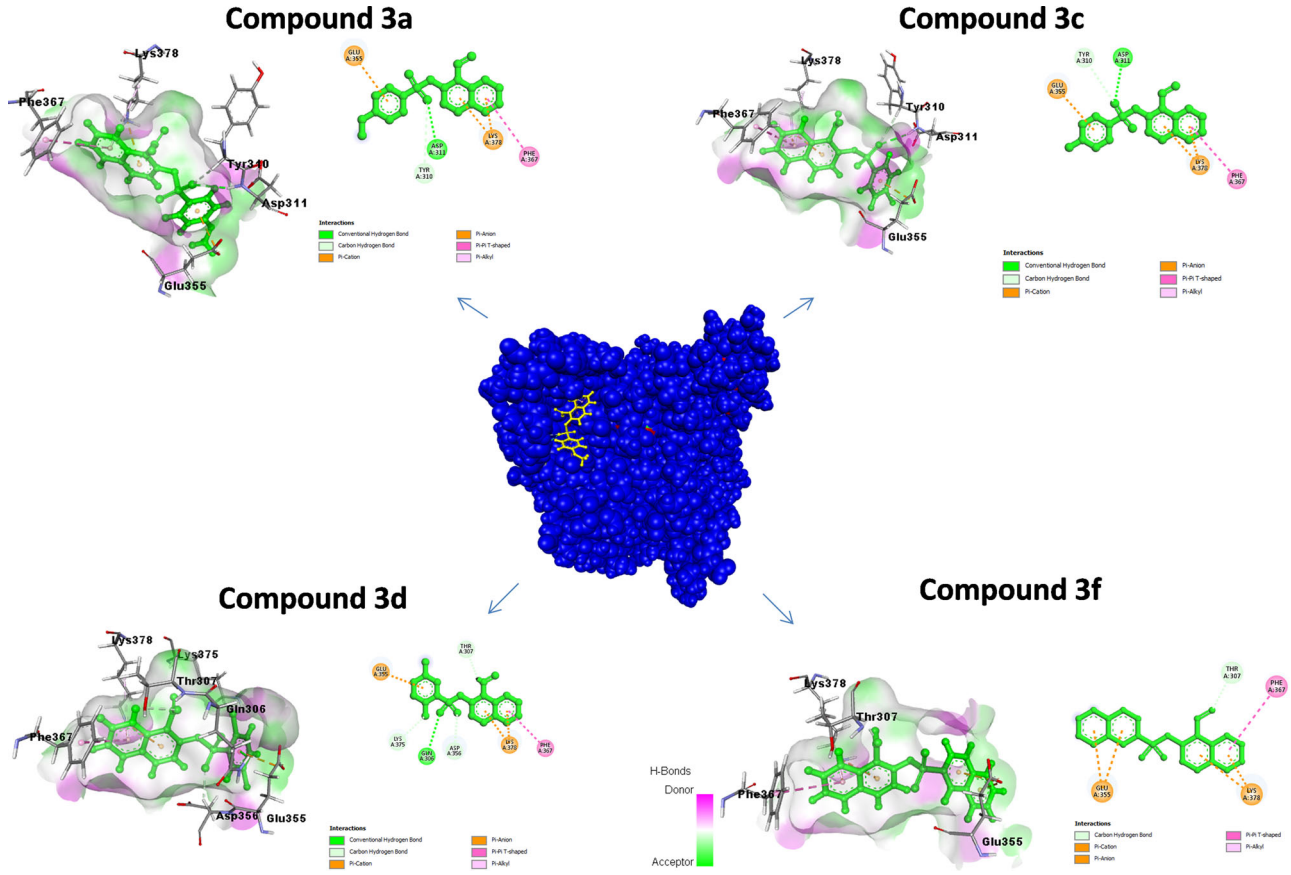

Figure 4. Hydrogen bond interactions and 2 D-structure poses of **3a**, **3c**, **3d**, and **3f** compounds with tyrosinase.

The interaction of compound **3d** with tyrosinase, unlike compounds **3a** and **3c**, depicted conventional hydrogen bond (GLN A:306) and carbon-hydrogen bond (ASP A:356, LYS A:375, and THR A:307) as hydrogen bond effects. The interaction of compound **3f** with tyrosinase showed the same interactions (electronic and hydrophobic) compared to compounds **3c** and **3d** except for all hydrogen bonds. The interactions of compounds **3a** and **3c** with tyrosinase, showed the same interaction as conventional hydrogen bonds (ASP A:311) like standard kojic acid. Similarly, the interaction of compound **3d** with tyrosinase exhibited the same interaction as conventional hydrogen bonds (GLN A:306) like kojic acid. The interaction of naphthalene-based sulfonate derivative **3f** with tyrosinase demonstrated the different interactions compared to kojic acid. The activity order of the compounds in the *in vitro* study was **3a** > **3c** = **3d** > **3f**. According to the *in silico* studies, the activity order was **3f** > **3c** > **3d** > **3a** for their best affinity values. Therefore, there is no compatibility between *in silico* and *in vitro* studies. Hydrogen bonding is the best interaction type of intermolecular interaction. When the compounds were compared in terms of hydrogen bond interaction in the molecular docking study, it was observed that compounds**3a**, **3c**, and **3d** interacted with the same amino acids as similar to kojic acid (ASP A: 311 for compounds **3a** and **3c**, GLN A: 306 for compound **3d**). In the hydrogen bond interaction, the strength of the interaction increases as the distance decreases. The hydrogen bond interaction distance of **3a**, **3c**, and kojic acid with the same amino acid (ASP A:311) were 2.681, 2.720, and 2.560 Å, respectively. Similarly, the hydrogen bond interaction distance of **3d** and kojic acid with the same amino acid (GLN A:306) were 2.999 and 2.348 Å, respectively. It is the least hydrogen bond interaction distance compound **3a** after the standard kojic acid. According to the hydrogen bond interaction effect, compound **3a** showed the best efficacy as it was found *in vitro* studies.

3.6.2. Molecular docking analysis of pancreatic lipase

The naphthalene-based sulfonate derivatives **(3a**, **3e**, **3 h**, and **3j)** were used to evaluate inhibition activity with pancreatic lipase (PDB ID:1ETH) obtained from the PDB server. The best affinity of the compounds**3a**, **3e**, **3 h**, and **3j** with pancreatic lipase exhibited −9.9, −8.6, −9.8, and −9.4 kcal/mol energies, respectively (Table 7). Among the investigated compounds, the best affinity value with pancreatic lipase was obtained with compound **3a** (−9.9 kcal/mol). The 2 D structure and hydrogen bond poses of the compounds with tyrosinase were demonstrated in Figure 5.

Using the molecular docking study, the most effective affinity value of orlistat (with pancreatic lipase) was found as −7.1 kcal/mol. The synthesized compounds (**3a**, **3e**, **3 h**, and **3j**) had a higher affinity value than the orlistat. The activity order of the compounds in the *in vitro* study was **3 h** > **3e** > **3j** > **3a**. Hence, the activity order of the compounds in the *in silico* studies was **3a** > **3h** > **3j** > **3e** according to the best affinity values. While compounds **3e, 3 h,** and

Table 6. Molecular docking data of tyrosinase.

Entry	Binding affinity (kcal/mol)	Type of ınteraction	Residue ınformation
3a	−8.0	Conventional hydrogen bond	ASP A:311
		Carbon hydrogen bond	TYR A:310
		Pi-Cation	LYS A:378
		Pi-Anion	GLU A:355
		Pi-Pi T-shaped	PHE A:367
		Pi-Alkyl	LYS A:378
3c	−8.5	Conventional hydrogen bond	ASP A:311
		Carbon hydrogen bond	TYR A:310
		Pi-Cation	LYS A:378
		Pi-Anion	GLU A:355
		Pi-Pi T-shaped	PHE A:367
		Pi-Alkyl	LYS A:378
3d	−8.3	Conventional hydrogen bond	GLN A:306
		Carbon hydrogen bond	ASP A:356; LYS A:375; THR A:307
		Pi-Cation	LYS A:378
		Pi-Anion	GLU A:355
		Pi-Pi T-shaped	PHE A:367
		Pi-Alkyl	LYS A:378
3f	−8.7	Carbon hydrogen bond	THR A:307
		Pi-Cation	LYS A:378
		Pi-Anion	GLU A:355
		Pi-Pi T-shaped	PHE A:367
		Pi-Alkyl	LYS A:378
Kojic acid	−5.1	Conventional hydrogen bond	GLN A: 306; ASP A:311; LYS A:375
		Amide-Pi Stacked	GLN A: 306

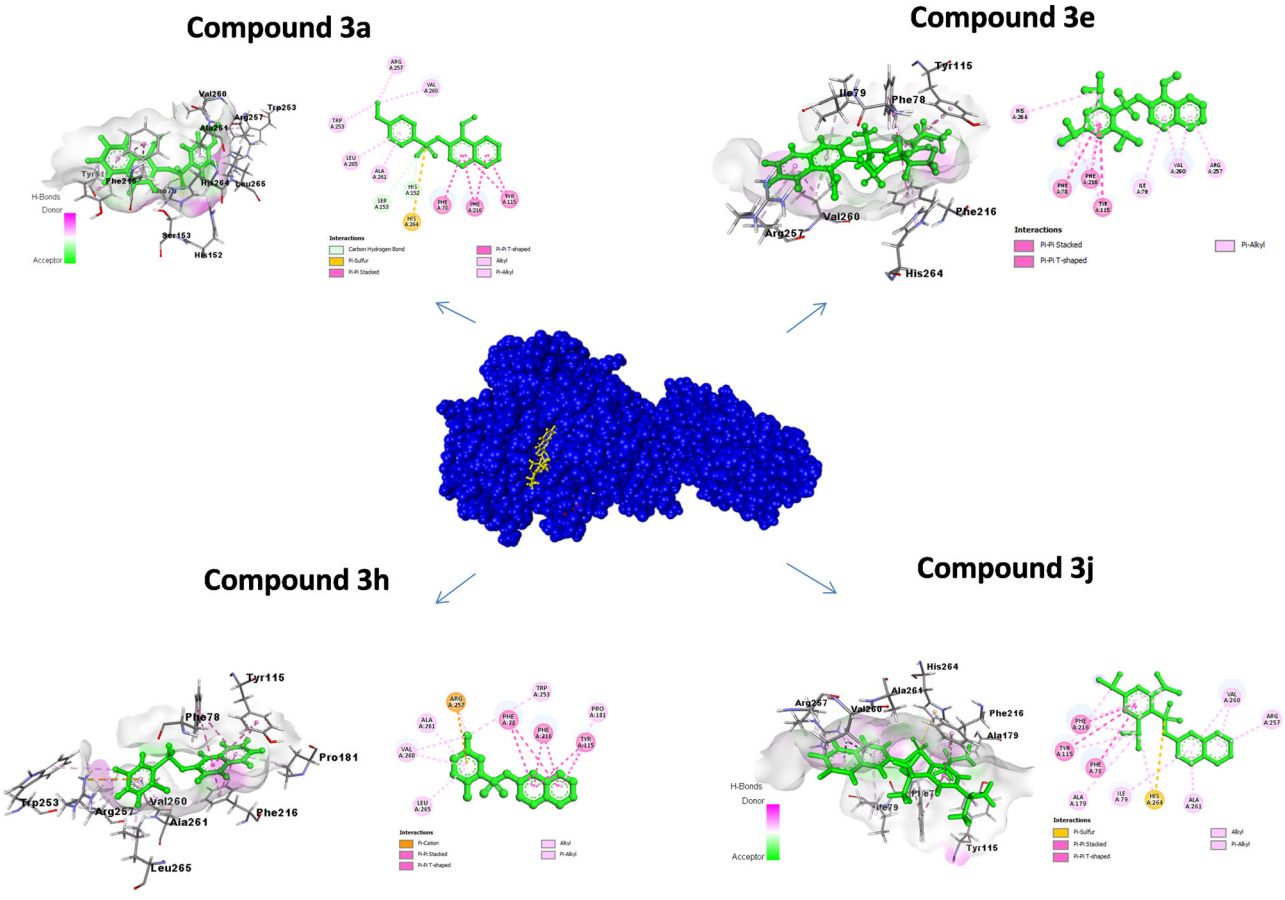

Figure 5. 2D-structure and H-bond poses of compounds **3a**, **3e**, **3 h**, and **3j** with pancreatic lipase.

3j did not have hydrogen bonding, compound **3a** had hydrogen bonding by binding to the same amino acid (HIS A: 152 and SER A:153) as the standard compound (orlistat). The hydrogen bond interaction distance of compound **3a** and orlistat with the same amino acid (HIS A:152) were 2.605 and 2.499 Å, respectively.

3.7. Druglikeness, ADME, and toxicity studies

ADME, druglikeness, physicochemical properties, and toxicity prediction of the naphthalene derivatives bearing functional sulfonate were performed by PreADMET and Molinspiration software (Lee et al., 2017; Molinspiration, 2011).

Table 7. Molecular docking data of pancreatic lipase.

Entry	Binding Affinity (kcal/mol)	Type of Interaction	Residue Information
3a	−9.9	Carbon hydrogen bond	HIS A:152; SER A:153
		Pi-Sulfur	HIS A:264
		Pi-Pi stacked	TYR A:115; PHE A:216
		Pi-Pi T-shaped	PHE A:78
		Alkyl	ARG A:257; VAL A:260
		Pi-Alkyl	TRP A:253; ALA A:261; LEU A:265
3e	−8.6	Pi-Pi stacked	TYR A:115; PHE A:216
		Pi-Pi T-shaped	PHE A:78
		Pi-Alkyl	PHE A:78;TYR A:115; PHE A:216; HIS A:264; ILE A:79; VAL A:260; ARG A:257
3h	−9.8	Pi-Cation	ARG A:257
		Pi-Pi Stacked	TYR A:115; PHE A:216
		Pi-Pi T-shaped	PHE A:78
		Alkyl	VAL A:260; ARG A:257
		Pi-Alkyl	TRP A:253; PRO A:181; VAL A:260; ARG A:257; ALA A:261; LEU A:265
3j	−10.1	Pi-Sulfur	HIS A:264
		Pi-Pi Stacked	TYR A:115; PHE A:216;
		Pi-Pi T-shaped	PHE A:78
		Alkyl	ALA A:179
		Pi-Alkyl	TYR A:115; PHE A:216; PHE A:78; HIS A:264; ILE A:79;VAL A:260; ALA A:261; ARG A:257
Orlistat	−7.1	Conventional Hydrogen Bond	GLY A:77; HIS A:152; SER A:153; ASP A:80
		Carbon-Hydrogen Bond	HIS A:152; HIS A:264; PHE A:78
		π-Sigma	PHE A:216
		Alkyl	PRO A:181; VAL A:260; ALA A:261; ARG A:257; LEU A:265; ILE A:79
		Pi-Alkyl	PHEA:78; TYRA:115; PHEA:216; TRPA:253

Table 8. Drug-likeness/ADME/toxicity prediction data of the compounds **3a-j**.

	Druglikeness/ADME/toxicity prediction of compounds (**1–10**)											
Entry	Rule of five	[a]Caco2	HIA	[b]BBB	Anes test	Carcino mouse	Carsino rat	hERG inhibition	[c]MDC K nm/s	Skin permeability	Buffer solubility (mg/L)	PPB
3a	suitable	18.977	98.141413	2.0285	mutagen	negative	negative	Low risk	0.7972	−1.67095	1.33918	100.0000
3b	suitable	13.022	97.474641	3.6311	mutagen	negative	negative	Low risk	1.0246	−1.64224	0.84832	99.69113
3c	suitable	5.853	97.553242	3.7605	mutagen	negative	negative	Low risk	0.0350	−1.52785	0.396468	97.20361
3d	suitable	14.575	97.616048	4.4706	mutagen	negative	negative	Medium risk	2.0655	−1.615	0.302424	100.0000
3e	suitable	21.524	97.592310	1.3182	Non-mutagen	negative	negative	Medium risk	0.0095	−0.85753	0.015209	93.34913
3f	suitable	18.771	97.621337	3.9171	mutagen	negative	negative	Low risk	0.7278	−1.55002	0.080296	100.0000
3g	suitable	20.962	97.397041	3.7066	mutagen	negative	negative	Low risk	0.8594	−1.65891	590.277	100.0000
3h	suitable	20.106	97.847957	3.3107	mutagen	negative	negative	Medium risk	2.6000	−1.4132	67.4147	98.79043
3i	suitable	21.501	97.510178	2.5790	mutagen	negative	negative	Medium risk	0.7797	−1.15909	106.803	100.0000
3j	suitable	21.826	97.821757	0.7563	Non-mutagen	negative	negative	Medium risk	0.7768	−0.743011	3.42553	96.82175

ADME = (Absorption, Distribution, Metabolism, and Excretion; HIA = Human Intestinal Absorption; BBB = Blood-Brain Barrier; MDCK = Madin-Darby Canine Kidney; PPB = Plazma Protein Binding.
[a]Caco2 > 70 is high, Caco2 = 4–70 is middle, and Caco2 < 4 is low.
[b]BBB> 0.40 is CNS-inactive and BBB < 0.40 is CNS-active.
[c]Permeability of MDCK values less than 25 nm/s are low, values ranging from 25 to 500 nm/s are medium, and values higher than 500 nm/s are high.

The obtained results of compounds **3a-j** are listed in Table 8. The HIA values obtained from PreADMET software were found as >70 for the compounds **3a-j** (Oja & Maran, 2018). It was determined that all compounds **3a-j** exhibited well absorption from the human intestinal absorption (HIA) from 70% to 100%. It was found that the Caco2 values of compounds **3a-j** demonstrated middle permeability (Caco2 > 70 is high, Caco2 = 4–70 is middle, and Caco2 < 4 is low) (Li et al., 2020). Also, BBB values of the compounds were found to be central nervous system (CNS)-inactive (Chen et al., 2021). Furthermore, skin permeability values of the compounds **3a-j** were observed as −1.67, −1.64, −1.52, −1.61, −0.85, −1.55, −1.65, −1.41, −1.15, and −0.74 cm/s, respectively. The log P values from −3 to +6 ensure the compounds have good absorption by the skin (Viana Nunes et al., 2020). According to the results, it was noted that all compounds have good absorption via the skin. In addition, the toxicity risk parameters were also calculated. The compounds were observed as mutagen except for **3e** and **3j**. The carcinogenicity mouse and rats were found to be negative. The hERG inhibition of the compounds demonstrated low risk except for compounds **3d**, **3e**, **3 h**, **3i**, and **3j**.

Absorbed percentage human intestinal absorption (HIA) from 0 to 20% are poor, from 20 to 70% are moderate, from 70 to 100% are high.

The compounds were calculated with low cell permeability (from 0.0298 to 3.4342 nm/s) for the MDCK. It has been reported that the bounding plasma protein bind (PPB) values < 90% are poor, and values > 90% are strong (Moussa et al., 2018). The observed results uncovered that all compounds'

Table 9. *In silico* physicochemical properties of the compounds **3a-j**.

Entry	M.W	miLog	TPSA	HBA	HBD	nrotB
3a	342.37	3.86	69.68	5	0	5
3b	346.79	4.48	60.45	4	0	4
3c	391.24	4.61	60.45	4	0	4
3d	381.24	5.09	60.45	4	0	4
3e	438.59	7.25	60.45	4	0	7
3f	362.41	4.99	60.45	4	0	4
3g	302.33	4.25	43.38	3	0	3
3h	353.23	5.37	43.38	3	0	3
3i	326.42	5.29	43.38	3	0	3
3j	410.58	7.53	43.38	3	0	6

MW = Molecular Weight; miLog = Octanol-water partition coefficient; TPSA = Total polar surface area; HBA = Hydrogen bond acceptor; HBD = Hydrogen bond donor; nrotB: Number of rotable bonds.

plasma protein bind (PPB) values exhibited strongly bounding (92–100). As a result, obeying Lipinski's rule of five, drug-likeness, physicochemical properties, and toxicity risk parameters of compounds **3a-j** were concluded to suitably predict pharmacokinetic values. In brief, the compounds can be drug candidates.

The Molinspiration software was utilized for the physiological properties of the naphthalene-based sulfonate derivatives **3a-j**, and the resulting data are exhibited in Table 9. The rule of five for drug-likeness properties of the compounds was suitable (less than five octanal-water partition coefficient (milogP) except compounds **3d**, **3e**, **3 h**, **3i**, and **3j** the molecular weight (M.W) less than 500 g/mol, less than five hydrogen bond donors (HBD), less than ten hydrogen bond acceptors (HBA), and less than ten rotatable bonds (nrotB). It was known that conventional oral drugs have topological polar surface areas (TPSA)of less than 140 Å (Whitty et al., 2017). According to preADMET studies, it was determined that TPSA values of compounds **3a-j** were less than 140 Å, meaning that they are similar to the drug-likeness. So, the compounds **3a-j** can be used as potential drug molecules relating to the drug-likeness.

4. Conclusıon

In this study, targeted naphthalene-based sulfonate derivatives were prepared by utilizing a TEA-mediated mild reaction process. Based on the obtained results, it was observed that naphthalene-based sulfonate derivatives showed suitable inhibitory activities against tyrosinase and pancreatic lipase enzymes compared to the standard inhibitors. Briefly, the enzyme assays showed that three of the synthesized compounds (**3a**, **3c**, and **3d**) had more effective inhibitions against the tyrosinase enzyme, whereas three other compounds (**3e**, **3 h**, and **3j**) had more effective inhibitions against the pancreatic lipase. The naphthalene-based sulfonate derivatives exhibited different effects on enzyme active sites owing to the interactions of different substituent groups. Based on the result of preADMET studies, it was observed that all compounds showed high HIA (70–100%) values. These values indicate that the compounds can be well absorbed for oral administration. The carcinogenicity mouse and rats were observed to be negative. Specifically, the hERG inhibition of the compounds **3a, 3 b**, **3c**, **3f**, and **3 g** demonstrated low risk. Furthermore, by establishing strong electrostatic interactions, such as hydrogen bonding and π-π stacking, a consistent charge distribution was found to be effective in contributing to the experimentally determined enzyme inhibition potential of the studied compounds against pancreatic lipase and tyrosinase. As a result, it can be said that these compounds can be used in *in vivo* studies and later as drugs.

Acknowledgment

The authors would like to thank the Eastern Anatolia High Technology Application and Research Center (DAYTAM) for HRMS and CHNS elemental analyses. The authors would like to thank the Mus Alparslan University Central Laboratory for the spectrometry analyses. The quantum chemical calculations reported in this paper were executed at TUBITAK ULAKBIM, High Performance and Grid Computing Center (TRUBA resources).

Disclosure statement

No potential conflict of interest was reported by the authors.

Funding

The author(s) reported there is no funding associated with the work featured in this article.

Authors contribution

Adem Korkmaz carried out the design, synthesis, analysis, enzyme inhibitions experiments, review, process, ADMET, molecular docking studies, writing and editing processes of the manuscript.

Gülbin Kurtay executed quantum chemical (DFT) calculations. She also contributed to the writing and editing processes of the manuscript.

Esin Kaya contributed to the chemical synthesis and editing of the article.

Ercan Bursal carried out the *in vitro* enzyme inhibition and *in silico* molecular docking studies and editing the paper.

ORCID

Adem Korkmaz http://orcid.org/0000-0002-0345-5794
Ercan Bursal http://orcid.org/0000-0001-7289-4507

References

Abbas, S., Nasir, H. H., Zaib, S., Ali, S., Mahmood, T., Ayub, K., Tahir, N. M., & Iqbal, J. (2018). Carbonic anhydrase inhibition of Schiff base derivative of imino-methyl-naphthalen-2-ol: Synthesis, structure elucidation, molecular docking, dynamic simulation and density functional theory calculations. *Journal of Molecular Structure*, *1156*, 193–200. https://doi.org/10.1016/j.molstruc.2017.11.086

Akocak, S., Taslimi, P., Lolak, N., Işık, M., Durgun, M., Budak, Y., Türkeş, C., Gülçin, İ., & Beydemir, Ş. (2021). Synthesis, characterization, and inhibition study of novel substituted phenylureidosulfaguanidine derivatives as α-glycosidase and cholinesterase inhibitors. *Chemistry & Biodiversity*, *18*(4), e2000958. https://doi.org/10.1002/cbdv.202000958

Alanazi, M. M., Elkady, H., Alsaif, N. A., Obaidullah, A. J., Alanazi, W. A., Al-Hossaini, A. M., Alharbi, M. A., Eissa, I. H., & Dahab, M. A. (2022). Discovery of new quinoxaline-based derivatives as anticancer agents and potent VEGFR-2 inhibitors: Design, synthesis, and in silico study. *Journal of Molecular Structure*, *1253*, 132220. https://doi.org/10.1016/j.molstruc.2021.132220

Ali, S. A., Awad, S. M., Said, A. M., Mahgoub, S., Taha, H., & Ahmed, N. M. (2020). Design, synthesis, molecular modelling and biological

evaluation of novel 3-(2-naphthyl)-1-phenyl-1H-pyrazole derivatives as potent antioxidants and 15-Lipoxygenase inhibitors. *Journal of Enzyme İnhibition and Medicinal Chemistry*, *35*(1), 847–863. https://doi.org/10.1080/14756366.2020.1742116

Aziz, H., Mahmood, A., Zaib, S., Saeed, A., El-Seedi, H. R., Pelletier, J., Sévigny, J., & Iqbal, J. (2021). Synthesis, characterization, alkaline phosphatase inhibition assay and molecular modelingstudies of 1-benzylidene-2-(4-tert-butylthiazol-2-yl) hydrazines. *Journal of Biomolecular Structure and Dynamics*, *39*(16), 6140–6153. https://doi.org/10.1080/07391102.2020.1802336

Aziz, H., Mahmood, A., Zaib, S., Saeed, A., Shafiq, Z., Pelletier, J., Sévigny, J., & Iqbal, J. (2020). Synthesis, characterization, in vitro tissue-nonspecific alkaline phosphatase (TNAP) and intestinal alkaline phosphatase (IAP) inhibition studies and computational evaluation of novel thiazole derivatives. *Bioorganic Chemistry*, *102*, 104088. https://doi.org/10.1016/j.bioorg.2020.104088

Behl, T., Kaur, D., Sehgal, A., Singh, S., Sharma, N., Zengin, G., Andronie-Cioara, F. L., Toma, M. M., Bungau, S., & Bumbu, A. G. (2021). Role of monoamine oxidase activity in Alzheimer's disease: An insight into the therapeutic potential of inhibitors. *Molecules*, *26*(12), 3724. https://doi.org/10.3390/molecules26123724

Biovia, Dassault Systèmes. (2017). "Discovery studio visualizer." San Diego, CA, USA 936.

Çakmak, R., Başaran, E., & Şentürk, M. (2022). Synthesis, characterization, and biological evaluation of some novel Schiff bases as potential metabolic enzyme inhibitors. *Archiv der Pharmazie*, *355*, e2100430.

Cetin, A., Türkan, F., Bursal, E., & Murahari, M. (2021). Synthesis, characterization, enzyme ınhibitory activity, and molecular docking analysis of a new series of thiophene-based heterocyclic compounds. *Russian Journal of Organic Chemistry*, *57*(4), 598–604. https://doi.org/10.1134/S107042802104014X

Chen, W., Yao, S., Wan, J., Tian, Y., Huang, L., Wang, S., Akter, F., Wu, Y., Yao, Y., & Zhang, X. (2021). BBB-crossing adeno-associated virus vector: An excellent gene delivery tool for CNS disease treatment. *Journal of Controlled Release*, *333*, 129–138. https://doi.org/10.1016/j.jconrel.2021.03.029

Ciupak, O., Daśko, M., Biernacki, K., Rachon, J., Masłyk, M., Kubiński, K., Martyna, A., & Demkowicz, S. (2021). New potent steroid sulphatase inhibitors based on 6-(1-phenyl-1 H-1, 2, 3-triazol-4-yl) naphthalen-2-yl sulphamate derivatives. *Journal of Enzyme Inhibition and Medicinal Chemistry*, *36*(1), 239–248. https://doi.org/10.1080/14756366.2020.1858820

Demir, Y., Taslimi, P., Koçyiğit, Ü. M., Akkuş, M., Özaslan, M. S., Duran, H. E., Budak, Y., Tüzün, B., Gürdere, M. B., Ceylan, M., Taysi, S., Gülçin, İ., & Beydemir, Ş. (2020). Determination of the inhibition profiles of pyrazolyl–thiazole derivatives against aldose reductase and α-glycosidase and molecular docking studies. *Archiv Der Pharmazie*, *353*(12), 2000118. https://doi.org/10.1002/ardp.202000118

Dennington, R., Keith, T., & Millam, J. (2009). GaussView, Version. GaussView, Version 5.0.8.

Elkady, H., Elwan, A., El-Mahdy, H. A., Doghish, A. S., Ismail, A., Taghour, M. S., Elkaeed, E. B., Eissa, I. H., Dahab, M. A., Mahdy, H. A., & Khalifa, M. M. (2022). New benzoxazole derivatives as potential VEGFR-2 inhibitors and apoptosis inducers: Design, synthesis, anti-proliferative evaluation, flowcytometric analysis, and in silico studies. *Journal of Enzyme Inhibition and Medicinal Chemistry*, *37*(1), 403–416. https://doi.org/10.1080/14756366.2021.2015343

Erdoğan, M., Polat Köse, L., Eşsiz, S., & Gülçin, İ. İ (2021). Synthesis and biological evaluation of some 1-naphthol derivatives as antioxidants, acetylcholinesterase, and carbonic anhydrase inhibitors. *Archiv Der Pharmazie*, *354*(8), 2100113. https://doi.org/10.1002/ardp.202100113

Frisch, M. J., Trucks, G. W., Schlegel, H. B., Scuseria, G. E., Robb, M. A., Cheeseman, J. R., Scalmani, G., Barone, V., Petersson, G. A., Nakatsuji, H., Li, X., Caricato, M., Marenich, A., Bloino, J., Janesko, B. G., Gomperts, R., Mennucci, B., Hratchian, H. P., Ortiz, J. V., … Fox, D. J. (2016). *Gaussian 09, Rev*. D.01, Gaussian Inc.

George, G., Auti, P. S., & Paul, A. T. (2021). Design, synthesis and biological evaluation of N-substituted indole-thiazolidinedione analogues as potential pancreatic lipase inhibitors. *Chemical Biology & Drug Design*, *98*(1), 49–59. https://doi.org/10.1111/cbdd.13846

Gümüş, M., Babacan, ŞN., Demir, Y., Sert, Y., Koca, İ., & Gülçin, İ. (2022). Discovery of sulfadrug–pyrrole conjugates as carbonic anhydrase and acetylcholinesterase inhibitors. *Archiv Der Pharmazie*, *355*(1), 2100242. https://doi.org/10.1002/ardp.202100242

Halder, A. K., Adhikary, N., Maity, M. K., & Jha, T. (2010). Synthesis, pharmacological activity and comparative QSAR modeling of 1, 5-N, N′-substituted-2-(substituted naphthalenesulphonyl) glutamamides as possible anticancer agents. *European Journal of Medicinal Chemistry*, *45*(5), 1760–1771. https://doi.org/10.1016/j.ejmech.2010.01.008

Hanwell, M. D., Curtis, D. E., Lonie, D. C., Vandermeersch, T., Zurek, E., & Hutchison, G. R. (2012). Avogadro: An advanced semantic chemical editor, visualization, and analysis platform. *Journal of Cheminformatics*, *4*(1), 17. https://doi.org/10.1186/1758-2946-4-17

Huo, P.-C., Hu, Q., Shu, S., Zhou, Q.-H., He, R.-J., Hou, J., Guan, X.-Q., Tu, D.-Z., Hou, X.-D., Liu, P., Zhang, N., Liu, Z.-G., & Ge, G.-B. (2021). Design, synthesis and biological evaluation of novel chalcone-like compounds as potent and reversible pancreatic lipase inhibitors. *Bioorganic & Medicinal Chemistry*, *29*, 115853. https://doi.org/10.1016/j.bmc.2020.115853

Kim, B. H., Park, K. C., Park, J. H., Lee, C. G., Ye, S. K., & Park, J. Y. (2016). Inhibition of tyrosinase activity and melanin production by the chalcone derivative 1-(2-cyclohexylmethoxy-6-hydroxy-phenyl)-3-(4-hydroxymethyl-phenyl)-propenone. *Biochemical and Biophysical Research Communications*, *480*(4), 648–654. https://doi.org/10.1016/j.bbrc.2016.10.110

Korkmaz, A. (2022). Synthesis, characterization, ADMET prediction and molecular docking studies of novel coumarinsulfonate derivatives. *Journal of the Institute of Science and Technology*, *12*, 918–932. https://doi.org/10.21597/jist.1089701

Korkmaz, A., & Bursal, E. (2022a). Synthesis, biological activity and molecular docking studies of novel sulfonate derivatives bearing salicylaldehyde. *Chemistry and Biodiversity*, *19*, e20220014.

Korkmaz, A., & Bursal, E. (2022b). Benzothiazolesulfonate derivatives bearing azomethine: Synthesis, characterization, enzyme inhibition, and molecular docking study. *Journal of Molecular Structure*, *1257*, 132641. https://doi.org/10.1016/j.molstruc.2022.132641

Korkmaz, A., & Bursal, E. (2022c). An in vitro and in silico study on the synthesis and characterization of novel bis (sulfonate) derivatives as tyrosinase and pancreatic lipase inhibitors. *Journal of Molecular Structure*, *1259*, 132734. https://doi.org/10.1016/j.molstruc.2022.132734

Korkmaz, A., Rhyman, L., & Ramasami, P. (2022). Synthesis, characterization, DFT and molecular docking studies of acetone O-((2,5-dichlorophenyl)sulfonyl) oxime. *Physical Sciences Reviews*. https://doi.org/10.1515/psr-2021-0230

Kumar, A., & Chauhan, S. (2021). Pancreatic lipase inhibitors: The road voyaged and successes. *Life Sciences*, *271*, 119115. https://doi.org/10.1016/j.lfs.2021.119115

Lee, S. K., Kang, Y., Chang, G. S., Lee, I. H., Park, S. H., & Park, J. (2017). Bioinformatics and molecular design research center. Yonsei University, Seoul https://preadmet.bmdrc.kr.

Li, S., Hu, X., Pan, J., Gong, D., & Zhang, G. (2021). Mechanistic insights into the inhibition of pancreatic lipase by apigenin: Inhibitory interaction, conformational change and molecular docking studies. *Journal of Molecular Liquids*, *335*, 116505. https://doi.org/10.1016/j.molliq.2021.116505

Liu, T. T., Liu, X. T., Chen, Q. X., & Shi, Y. (2020). Lipase inhibitors for obesity: A review. *Biomedicine & Pharmacotherapy = Biomedecine & Pharmacotherapie*, *128*, 110314. https://doi.org/10.1016/j.biopha.2020.110314

Li, Y., Xu, Y., Pan, C., Ren, Z., & Yang, X. (2020). TRIF is essential for the anti-inflammatory effects of Astragalus polysaccharides on LPS-infected Caco2 cells. *International Journal of Biological Macromolecules*, *159*, 832–838. https://doi.org/10.1016/j.ijbiomac.2020.05.005

Maya, A. B. S., Pérez-Melero, C., Mateo, C., Alonso, D., Fernández, J. L., Gajate, C., Mollinedo, F., Peláez, R., Caballero, E., & Medarde, M. (2005). Further naphthylcombretastatins.An investigation on the role of the naphthalene moiety. *Journal of Medicinal Chemistry*, *48*(2), 556–568. https://doi.org/10.1021/jm0310737

Menteşe, E., Yı lmaz, F., Emirik, M., Ülker, S., & Kahveci, B. (2018). Synthesis, molecular docking and biological evaluation of some

benzimidazole derivatives as potent pancreatic lipase inhibitors. *Bioorganic Chemistry*, *76*, 478–486. https://doi.org/10.1016/j.bioorg.2017.12.023

Mirzazadeh, R., Asgari, M. S., Barzegari, E., Pedrood, K., Mohammadi-Khanaposhtani, M., Sherafati, M., Larijani, B., Rastegar, H., Rahmani, H., Mahdavi, M., Taslimi, P., Üç, E. M., & Gulçin, İ. (2021). New quinoxalin-1, 3, 4-oxadiazole derivatives: Synthesis, characterization, in vitro biological evaluations, and molecular modeling studies. *Archiv Der Pharmazie*, *354*(9), 2000471. https://doi.org/10.1002/ardp.202000471

Molinspiration, C. (2011). http://www.molinspiration.com/cgi-bin/properties.

Moussa, G., Alaaeddine, R., Alaeddine, L. M., Nassra, R., Belal, A. S. F., Ismail, A., El Yazbi, A. F., Abdel, Ghany, Y. S., & Hazzaa, A. (2018). Novel click modifiable thioquinazolinones as anti-inflammatory agents: Design, synthesis, biological evaluation and docking study. *European Journal of Medicinal Chemistry*, *144*, 635–650. https://doi.org/10.1016/j.ejmech.2017.12.065

Oja, M., & Maran, U. (2018). pH-permeability profiles for drug substances: Experimental detection, comparison with human intestinal absorption and modelling. *European Journal of Pharmaceutical Sciences*, *123*, 429–440. https://doi.org/10.1016/j.ejps.2018.07.014

Pettersen, E. F., Goddard, T. D., Huang, C. C., Couch, G. S., Greenblatt, D. M., Meng, E. C., & Ferrin, T. E. (2004). UCSF Chimera—A visualization system for exploratory research and analysis. *Journal of Computational Chemistry*, *25*(13), 1605–1612. https://doi.org/10.1002/jcc.20084

Pillaiyar, T., Manickam, M., & Namasivayam, V. (2017). Skin whitening agents: Medicinal chemistry perspective of tyrosinase inhibitors. *Journal of Enzyme İnhibition and Medicinal Chemistry*, *32*(1), 403–425. https://doi.org/10.1080/14756366.2016.1256882

Schrödinger LLC. (2021). The PyMOL molecular graphics system, version 2.5.2.

Shirinzadeh, H., Dilek, E., & Alım, Z. (2022). Evaluation of naphthalenylmethylen hydrazine derivatives as potent ı nhibitors on, antiatherogenic enzymes, paraoxonase ı and acetylcholinesterase activities. *ChemistrySelect*, *7*(5), e202104489. https://doi.org/10.1002/slct.202104489

Song, X., Ni, M., Zhang, Y., Zhang, G., Pan, J., & Gong, D. (2021). Comparing the inhibitory abilities of epigallocatechin-3-gallate and gallocatechingallate against tyrosinase and their combined effects with kojic acid. *Food Chemistry*, *349*, 129172. https://doi.org/10.1016/j.foodchem.2021.129172

Trott, O., & Olson, A. J. (2010). Software news and update AutoDockVina: İmproving the speed and accuracy of docking with a new scoring function. efficient optimization, and multithreading. *Journal of Computational Chemistry*, *31*(2), 455–461. https://doi.org/10.1002/jcc.21334

Turkan, F., Cetin, A., Taslimi, P., Karaman, H. S., & Gulcin, I. (2019). Synthesis, characterization, molecular docking and biological activities of novel pyrazoline derivatives. *Archiv Der Pharmazie*, *352*(6), 1800359. https://doi.org/10.1002/ardp.201800359

Viana Nunes, A. M., das Chagas Pereira de Andrade, F., Filgueiras, L. A., de Carvalho Maia, O. A., Cunha, R. L. O. R., Rodezno, S. V. A., Maia Filho, A. L. M., de Amorim Carvalho, F. A., Braz, D. C., & Mendes, A. N. (2020). preADMET analysis and clinical aspects of dogs treated with the Organotellurium compound RF07: A possible control for canine visceral leishmaniasis? *Environmental Toxicology and Pharmacology*, *80*, 103470.

Wang, G., Liu, W., Tang, J., Ma, X., Gong, Z., Huang, Y., Li, Y., & Peng, Z. (2020). Design, synthesis, and anticancer evaluation of benzophenone derivatives bearing naphthalene moiety as novel tubulin polymerization inhibitors. *Bioorganic Chemistry*, *104*, 104265. https://doi.org/10.1016/j.bioorg.2020.104265

Whitty, A., Viarengo, L. A., & Zhong, M. (2017). Progress towards the broad use of non-peptide synthetic macrocycles in drug discovery. *Organic & Biomolecular Chemistry*, *15*(37), 7729–7735. https://doi.org/10.1039/c7ob00056a

Yetişsin, F., & Kardeş, İ. (2022). Could acetone O-(4-chlorophenylsulfonyl) oxime be a copper chelating and antioxidative molecule on maize seedlings? *International Journal of Phytoremediation*, *24*(7), 721–729. https://doi.org/10.1080/15226514.2021.1970101

Yuriev, E., Agostino, M., & Ramsland, P. A. (2011). Challenges and advances in computational docking: 2009 in review. *Journal of Molecular Recognition: JMR*, *24*(2), 149–164. https://doi.org/10.1002/jmr.1077

Zhang, J., Yang, Y., Qian, X.-K., Song, P.-F., Zhao, Y.-S., Guan, X.-Q., Zou, L.-W., Bao, X., & Wang, H. (2021). Design, synthesis, and structure-activity relationship study of pyrazolones as potent ınhibitors of pancreatic lipase. *ChemMedChem*. *16*(10), 1600–1604. https://doi.org/10.1002/cmdc.202000850

Zolghadri, S., Bahrami, A., Hassan Khan, M. T., Munoz-Muno, J., Garcia-Molina, F., Garcia-Canovas, F., & Saboury, A. A. (2019). A comprehensive review on tyrosinase inhibitors. *Journal of Enzyme İnhibition and Medicinal Chemistry*, *34*(1), 279–309. https://doi.org/10.1080/14756366.2018.1545767